学 位 論 文

Analysis of the effect of parathyroid hormone (PTH) treatment on osteoblastogensis from leptin receptor-positive mesenchymal stem cells

Mengyu Yang

Department of Hard Tissue Research, Graduate School of Oral Medicine
（Chief Academic Advisor: Professor Nobuyuki Udagawa）

The thesis submitted to the Graduate School of Oral Medicine,
Matsumoto Dental University, for the degree Ph.D. (in Dentistry)

Analysis of the effect of parathyroid hormone (PTH) treatment on osteoblastogensis from leptin receptor-positive mesenchymal stem cells

「副甲状腺ホルモンによる Leptin 受容体陽性間葉系幹細胞の骨芽細胞分化機構の解析」

CONTENTS

ABBREVIATION

ALP	Alkaline phosphatase
BAC	Bacterial artificial chromosome
Bglap	Bone gamma-carboxyglutamic acid-containing protein
BM	Bone marrow
BM-MSPCs	Bone marrow mesenchymal stem and progenitor cells
BV/TV	Bone volume over total volume
CAR	CXCL12 abundant reticular
Cebpβ	CCAAT enhancer-binding protein-β
CFU-F	Colony-forming unit-fibroblasts
Col1(2.3)	type I Collagen α (2.3)
CXCL12	CXC chemokine ligand 12
EdU	5-ethynyl-2'-deoxyuridine
FABP4	Fatty acid binding protein 4
FACS	Fluorescence-activated cell sorter
hPTH (1-34)	Amino acid 1-34 fragment of human PTH
LepR	Leptin Receptor
μCT	Micro-computed tomography
ML-cells	Mutilayered cells
Nes	Nestin
Osx	Osterix
OVX	Ovariectomized
PFA	Paraformaldehyde
PDGFRα	Platelet-derived growth factor receptor α
PI	Propidium iodide
PPARγ	Peroxisome proliferator-activated receptor γ
PTHrP	PTH/PTH-related peptide
RNA-seq	RNA sequencing
Runx2	Runt-related transcription factor 2
SD	Standard deviation
Tb.N.	Trabecular number
Tb.Th.	Trabecular thickness

Tb.Sp.	Trabecular separation
VE-Cad	VE-cadherin
VEGF-A	Vascular endothelial growth factor A
Zfp467	Zinc finger protein 467
3D	Three-dimensional
5-FU	5-Fluorouracil

Chapter 1

1. ABSTRACT

Bone marrow mesenchymal stem and progenitor cells (BM-MSPCs) maintain homeostasis of bone tissue by providing osteoblasts. Although several markers have been identified for labeling of MSPCs, these labeled cells still contain non-BM-MSPC populations. Studies have suggested that MSPCs are observed as leptin receptor (LepR)-positive cells, whereas osteoblasts can be classified as positive for Runx2, a master regulator for osteoblastogenesis. Here, we demonstrate, using Runx2-GFP reporter mice, that the LepR-labeled population contains Runx2-GFP^{low} sub-population, which possesses higher fibroblastic colony-forming units (CFUs) and mesensphere capacity, criteria for assessing stem cell activity, than the Runx2-GFP^{-} population. In response to parathyroid hormone (PTH), a bone anabolic hormone, LepR^{+}Runx2-GFP^{low} cells increase Runx2 expression and form multilayered structures near the bone surface. Subsequently, the multilayered cells express Osterix and Type I collagen α, resulting in generation of mature osteoblasts. Therefore, our results indicate that Runx2 is weakly expressed in the LepR^{+} population without osteoblastic commitment, and the LepR^{+}Runx2-GFP^{low} stromal cells sit atop the BM stromal hierarchy.

2. INTRODUCTION

Bone marrow (BM) cells belonging to mesenchymal lineages are derived from mesenchymal stem and progenitor cells (MSPCs). BM-MSPCs are traditionally characterized as cells possessing colony forming potential in adherent culture conditions [known as colony-forming unit-fibroblasts, CFU-F] and have the ability to form clonal spheres in nonadherent culture conditions [designated as mesenspheres][1-3]. The clonally expanded CFU-F colonies and mesenspheres have differentiation potential to osteoblasts, adipocytes and chondrocytes both *in vitro* and *in vivo*. BM-MSPCs can be marked by the expression of leptin receptor (LepR)-Cre, and are distributed nearby blood vessels throughout the whole BM cavity [4-6]. *In vivo* fate mapping approaches demonstrated that $LepR^+$ cells differentiate to osteoblasts and adipocytes under normal conditions. The contribution of $LepR^+$ cells to chondrocytes is observed during the healing process of bone tissue [5,6]. There is evidence that LepR-Cre-labeled cells largely overlap with other markers for the BM-MSPC populations including $CD31^-CD45^-Ter119^-Nestin\text{-}GFP^{low}$ cells [5,7], CXCL12 abundant reticular (CAR) cells [8,9], $PDGFR\beta^+$ cells [5,6] and Prx-1-Cre labeled cells [10]. Although these markers make it possible to enrich the BM-MSPCs from whole BM cells, not all the labeled cells have the potential to form CFU-F colonies or clonal mesenspheres [6,7,11]. These results suggest that the fractions are impure and still contain non-BM-MSPC populations.

Runt-related transcription factor 2 (Runx2) is a master regulator for osteoblast differentiation [12-14]. Osteoblastogenesis is fully suppressed by the global knockout of Runx2 [13,14]. Exon 8 of Runx2 gene conditional deletion in mature osteoblasts, which express Cre recombinase under the control of a 2.3-kb fragment of the type I collagen α [(Col1(2.3)] promoter, exhibit low bone mass phenotype [15]. In contrast, conditional knockout mice lacking exon 4 of Runx2 gene in mature osteoblasts have no effect on osteoblastic activity [16]. These studies indicate that the necessity of Runx2 in osteoblastic activity is still controversial. On the other hand, *in vivo* lineage tracing studies have demonstrated that Runx2 is essential for osteoblast lineage commitment [17]. Interestingly, Runx2 overexpression approaches

revealed that the late stage of osteoblastogenesis is negatively regulated by Runx2, whose levels were found to decrease with osteoblast maturation [18,19]. Overall, these findings suggest that Runx2 is required for osteoblast commitment from immature mesenchymal stromal cells. These results raise the intriguing possibility that Runx2 may be expressed in a portion of $LepR^+$ stromal cells, which have osteogenic-committed sub-populations.

Osteoblastogenesis is completely diminished in knockout mice lacking Osterix (Osx), a transcription factor that acts downstream of Runx2 [20]. Furthermore, bone formation is inhibited by conditionally deleting Osx in mature osteoblasts [21]. These results suggest that Osx is necessary not only for osteoblast differentiation, but also for their functions. On the other hand, during endochondral bone ossification, BM-MSPCs are generated from part of the developing chondrogenic cell populations [17]. The expression levels of Osx are increased throughout the development of chondrogenic cell populations that subsequently differentiate into BM-MSPCs [5,17,22]. Although Osx protein expression in BM-MSPCs is completely lost in the adult stage, mRNA expression is maintained [15,23]. However, the Osx expression pattern during osteoblastogenesis from BM-MSPCs has yet to be elucidated.

Teriparatide, a biologically active amino acid 1–34 fragment of human PTH [hPTH (1–34)], is clinically used in treatment of osteoporosis patients [24]. Several studies have demonstrated that intermittent PTH treatment induces remedial action against osteoporosis due to anabolic effects on bone tissue [25-28]. Researchers have found that osteoblast precursors are increased along the bone surfaces in response to PTH treatment [27-30]. These results suggest that the anabolic effects of PTH on bone tissue are exerted by the acceleration of osteoblastogenesis from immature BM mesenchymal precursors. However, it still remains unclear which BM stromal cells give rise to osteoblasts in response to PTH treatments, thereby mediating the therapeutic response in osteoporosis.

Here we demonstrate, using Runx2-GFP reporter mice, that the $LepR^+$ cell population contains Runx2-GFP^{low} cells, and unexpectedly, that stem cell capacity is enriched in the Runx2-GFP^{low} sub-population. In addition, our studies have shown

that the LepR^{+}Runx2-GFP^{low} cells differentiate into mature osteoblasts via multilayered cell formation adjacent to bone surfaces in response to PTH-induced bone anabolic effects. These results provide evidence that LepR^{+}Runx2-GFP^{low} cells sit atop the BM mesenchymal stromal cell hierarchy.

3. EXPERIMENTAL PROCEDURES

3.1 Experimental Animals.

C57BL/6, B6.129-Lepr*tm2(cre)Rck*/J (LepR-*Cre*), B6.Cg-*Gt(ROSA)26Sortm14 (CAG-tdTomato)Hze*/J mice were purchased from Jackson Laboratory (Bar Harbor, ME). Osx-Cre^{ERT2} mice [34] were provided from H.M. Kronenberg (Endocrine Unit, Massachusetts General Hospital and Harvard Medical School, USA). Col1(2.3)-*Gfp* mice [45] and Runx2-*Gfp* mice [31] were generated in one of the author's laboratories, and backcrossed with C57BL/6 (SLC, Shizuoka, Japan) for 5 generations. 5–7 week-old mice were used for all experiments. All mice were maintained in pathogen-free conditions in animal facilities certified by the Animal Care and Use Committees of Matsumoto Dental University, and animal protocols were approved by that committee. All animal studies were performed in accordance with the Guidelines of the Matsumoto Dental University Animal Care Committee.

3.2 Antibodies and reagents.

The primary antibodies used were Alexa Fluor 647-anti-VE-Cadherin and Alexa Fluor 647-anti-CD31/PECAM-1 (MEC13.3) (all from Biolegend, San Diego, CA); APC or PE-anti-CD45 (30-F11), APC or PE-anti-Ter119 (Ter119) (all from eBioscience, Waltham, MA); anti-LepR, anti-SOST/Sclerostin and anti-fatty acid binding protein 4 (FABP4) (all from R&D systems, Minneapolis, MN); anti-Osteocalcin (R21C-01A) and anti-DMP-1 (all from TAKARA, Shiga, Japan);anti-Perilipin (Novus Biologicals, Centennial, CO); anti-chick type II collagen (A2-10) (Chondrex); anti-Runx2 (D1L7F) (Cell Signaling, Danvers, MA). The secondary antibodies used were Alexa Fluor 647 donkey anti-goat IgG and Alexa Fluor 594 donkey anti-rat IgG (all from Molecular probes, Waltham, MA); Cy3 donkey anti-mouse IgG (Merck Millipore, Burlington, MA); FITC donkey anti-rabbit IgG (Bethyl Laboratories, Montgomery, TX). Alexa Fluor 488-anti-GFP (Molecular Probes) was used for enhancement of the Runx2-GFP signal. Nuclei were stained with Hoechst 33342 (Sigma-Aldrich, St. Louis, MO) or TO-PRO-3 Iodide (642/661) (Molecular Probes).

3.3 PTH treatment and induction of Cre-mediated recombination.

Human PTH (1–34) was kindly provided from Asahi Kasei Pharma Co. Ltd (Tokyo, Japan). Four-six-week-old mice were intraperitoneally injected with PTH (80 μg/kg/12 hours) for 10 days. Forty-eight hours after the final PTH injection, mice were sacrificed and used for analyses. For induction of Cre-mediated recombination in Osx-Cre^{ERT2} mice, CRF-1 chow diet (Oriental Yeast, Tokyo, Japan) containing tamoxifen (Sigma-Aldrich) at 400 mg/kg was given from 5 days before the first PTH injection until the end of the experiment.

3.4 Microscopy imaging.

Mice were perfused with 4% paraformaldehyde (PFA) for fixation, and bone tissue were further fixed with 4% PFA for 24 hours at 4 ℃, and incubated in 10%, 20% and 30% sucrose each for 2 hour sat 4 ℃ for cryoprotection, then embedded in 5% carboxymethyl cellulose (SECTION-LAB, Hiroshima, Japan). Sections, 10–20-μm thick, were prepared using Kawamoto's film method[46]. Z-stack confocal projection images were obtained from 2-μm interval images from 10–20-μm thick sections. Fluorescence and phase-contrast images were acquired using a laser-scanning confocal microscope (LSM510, Carl Zeiss, Oberkochen, Germany) equipped with Plan-Apochromat (10×/0.45 and 20×/0.8), ZEN and Axiovision software (Carl Zeiss). Bright-field images were acquired using a Light microscope Zeiss Axiovert 200 (Carl Zeiss) equipped with Plan-NEOFLUAR (2.5×/0.075), LD A-plan (40×/0.50 Ph2) and Axiovision software (Carl Zeiss) and Stemi 2000-C (Carl Zeiss).

3.5 Preparation of BM cell suspension.

BM was gently flushed in L-15 FACS buffer [47]. BM was digested with 0.1% collagenase IV (Gibco, Waltham, MA), 0.2% Dispase (Gibco) and 20 U/ml DNase (Worthington Biochemical, Lakewood, NJ) in HBSS (Gibco) for 30 min at 37 ℃.

3.6 CFU-F assay.

Mouse sorted cells were seeded at 2–3 ×10^3 cells per well in a 12-well adherent tissue cultureplate using a MesenCult proliferation Kit with MesenPure (StemCell Technologies, Vancouver, BC) containing 100 U/ml and 100 μg/ml penicillin-streptomycin. Half of the media was replaced after 7 days and at day 10, cells were

stained with Giemsa staining solution (EMD Chemicals, Darmstadt, Germany) and adherent colonies were counted.

3.7 Spheroid formation assay.

Mouse sorted cells at 1×10^3 were transferred to non-adherent 24 well plates (Corning, NY, USA) with spheroid-forming media [5, 7, 47] [1:2 ratio of DMEM F12 (Gibco) and Human Endothelial Medium (Gibco) supplemented with 3.75% Chicken Extract (US Biological, Salem, MA), 0.1 mM β-ME (Invitrogen, Waltham, MA), 1% Non-essentialamino acids (Gibco), 1% Pen-strep (Gibco), 1% N2 (Gibco), 2% B27 (Gibco), 20 ng/mL human bFGF (R&D systems), 20 ng/mL mouse PDGF (Peprotech, Rocky Hill, NJ), 20 ng/mL mouse oncostatin M (R&D systems), 20 ng/mL mouse IGF-1 (Peprotech), 20 ng/mL mouse EGF (Peprotech)]. After 7 days, the spheroid efficiency was determined.

3.8 Cell sorting and flow cytometry.

Cell sorting experiments were performed using an Aria III Cell Sorter (BD Biosciences, San Jose, CA). Flow cytometric analyses were carried out using a Cytomics FC 500 flow cytometer equipped with CXP software (all Beckman Coulter Life Sciences, Brea, CA). Dead cells and debris were excluded by FSC, SSC, DAPI (Dojindo, Kumamoto, Japan) and Fixable Viability Dye eFluor 780 (eBioscience) staining profiles. Data were analysed with FlowJo (Tree Star, Ashland, OR) software.

3.9 *In vitro* cell differentiation.

Sorted LepR-Cre/Tomato$^+$Runx2-GFP^{low} stromal cells were expanded using a MesenCult proliferation Kit with MesenPure (StemCell Technologies) containing 100 U/ml and 100 μg/ml penicillin-streptomycin. Osteogenic, adipogenic and chondrogenic differentiation were induced using a Mouse Mesenchymal Stem Cell Function Identification Kit (R&D systems). Cells were maintained with 5% CO_2 in a water-jacketed incubator at 37 ℃ for 2-5 weeks. Mineralized osteogenic cells were identified by Alizarin Red S (Sigma-Aldrich) staining. Adipocytes were identified by characteristic production of lipid droplets and staining with an anti-FABP antibody (R&D systems). Chondrocytic cells were identified using an Alcian Blue 8GX solution (Sigma-Aldrich).

3.10 RNA isolation and quantitative real-time PCR.

Sorted cells were collected in TRIzol reagent (Ambion, Waltham, MA) and mRNA was purified using a PureLink RNA Micro kit (Invitrogen). Reverse transcription and quantitative real-time PCR were performed using a One Step SYBR Prime Script PLUS RT-PCR kit (TAKARA, Shiga, Japan) and an Applied Biosystems StepOnePlus™ (Applied Biosystems, Waltham, MA). Gene expression data was normalized to *Gapdh*. The sequences of primers for each gene were as follows:

	Forward	Reverse
Gapdh	TGTGTCCGTCGTGGATCTGA	TTGCTGTTGAAGTCGCAGGAG
PDGFRa	AGCAAACATCTTGAC TTGGGAACA	ACTTGCATCATTCCCGGACAC
CXCL12	CCAGAGCCAACGTCAAGCAT	CAGCCGTGCAACAA TCTGAA
LepR	TCAGAATTTTGGGTGGAAAA	GTCCAGGTGAGGAGCAAGAG
Runx2	CCAGCCACCGAGACCAACC	CCAGCCACCGAGACCAACC

3.11 Microcomputed tomography analysis.

Femora were fixed in 70% ethanol. Three-dimensional (3D) reconstructions of distal femora were obtained by micro-computed tomography (μCT) (ScanXmate-A080,Comscan Tecno, Kanagawa, Japan). Morphological indices were calculated in trabecular bones located from 0.5 to 1.5 mm from the growth plates using image analysis software (TRI/3D-BON, Ratoc Syatem Engineering, Tokyo, Japan).

3.12 Statistics.

The results were expressed as mean ± SD. Data were evaluated by unpaired Student's *t*-tests. Experiments were performed three times and similar results were obtained. Statistical analyses were performed with GraphPad Prism 6 (GraphPad Softwear Inc., La Jolla, CA). $P < 0.05$ was considered significant.

4. RESULTS

4.1 Runx2 is heterogeneously expressed in the LepR$^+$ BM stromal cell population.

To detect Runx2 expressing cells in bone tissue, we analyzed Runx2-GFP reporter mice, in which GFP is driven by a bacterial artificial chromosome (BAC) of Runx2 locus [31]. FITC-conjugated anti-GFP antibody was used to amplify the intensity of the GFP signal when imaging bone tissue sections. Consistent with a previous study [31], Runx2-GFP$^+$ expression in bone tissues was detected in osteoblasts, osteocytes and chondrocytes (Fig. 1A–D). Interestingly, the Runx2-GFP signal was observed not only in bone tissues, but also in the BM cavity (Fig. 1A, right panel). Some hematopoietic cells were observed as GFP-positive cells due to nonspecific binding of the anti-GFP antibody (compare wild-type and Runx2-GFP mice in Fig. 1E). On the other hand, VE-cadherin (VE-Cad) and CD31-positive endothelial cells, and Perilipin-positive adipocytes did not express Runx2-GFP (Fig. 1F,G). It is interesting to note that leptin receptor-positive (LepR$^+$) BM stromal cells, which are considered to have characteristics of BM-MSPCs, also weakly expressed Runx2-GFP throughout the bone marrow cavity (Fig. 1H). These results indicate that the osteoblastic master regulator Runx2 may already be expressed in the pre- or early osteoblastic lineage-committed LepR$^+$ sub-population.

To further analyze Runx2-GFP expression pattern in the BM stromal population, we performed flow cytometric analyses of BM cells in the Runx2-GFP mice. Runx2-GFP$^+$ cells were observed in the BM stromal cell population without enhancing the GFP signal by FITC-conjugated anti-GFP antibody (Fig. 2A). We found two distinct types of Runx2-GFP$^+$ cells on the basis of their GFP expression levels and cellular morphology (designated as Runx2-GFP^{low} and -GFP^{high} cells) (Fig. 2A). Most of the Runx2-GFP^{low} cells (82.0 ± 1.4%), but not Runx2-GFP^{high} cells (3.3 ± 1.8%), were positive for LepR (Fig. 2A). Previous reports suggested that mature osteoblasts are negative for LepR [5, 6]. These results indicate that the mature osteoblasts are contained in the Runx2-GFP^{high} population. Next, we analyzed the Runx2-GFP expression pattern in LepR$^+$ cells. Interestingly, most of the LepR$^+$ cells were positive for Runx2-GFP (64.6 ± 2.0%) (designated as LepR$^+$Runx2-GFP^{low} cells)

(Fig. 2B, right panel). The frequency and absolute number of LepR$^+$Runx2-GFP^{low} cells per femur were approximately 3-times higher than those of LepR$^+$Runx2-GFP$^-$ cells (Fig. 2C,D). These results indicate that LepR$^+$ cells consist of two populations: LepR$^+$Runx2-GFP^{low} and LepR$^+$Runx2-GFP$^-$ sub-populations.

4.2 Stem cell activity is enriched in the Runx2-GFP^{low} sub-population of LepR$^+$ cells.

Upregulation of Runx2 expression is thought to indicate osteoblastic commitment of multipotent BM stromal progenitors [32].We next generated LepR-Cre/ROSA26-loxP-stop-loxP-tdTomato/Runx2-GFP (LepR/Tomato/Runx2-GFP) mice, and analyzed whether stem cell activity in LepR$^+$ cells increases in inverse proportion to Runx2 expression levels. Previous reports demonstrated that the differentiation of LepR$^+$ cells into mature osteoblasts is mainly observed in adult mice, and only rarely seen in young mice [5, 6]. In order to avoid contamination of the LepR-Cre-labeled population with LepR$^+$ cell-derived osteoblasts, we analyzed young mice (5–7 weeks old) in this experiment. Histological analysis demonstrated that bone-lining osteoblasts were strongly positive for Runx2-GFP, but negative for LepR/Tomato (Fig. 3A, asterisks). These results indicate that LepR-Cre-labeled Tomato$^+$ (LepR/Tomato$^+$) cells do not contain the osteoblastic population in young mice. On the other hand, the LepR/Tomato$^+$ cells in the BM cavity were positive for Runx2-GFP (Fig. 3A, arrows). Immunofluorescence staining showed that LepR/Tomato$^+$ cells express Runx2 protein (Fig. 3B, arrows). Flow cytometric analysis also demonstrated that the majority of LepR/Tomato$^+$ cells in BM expressed Runx2-GFP (60.9 ± 2.5%) (Fig. 3C). We then assessed the stem cell activity of both Runx2-GFP^{low} and Runx2-GFP$^-$ sub-populations in LepR/Tomato$^+$ cells by performing CFU-F assays of cell sorted BM stromal fractions (Fig. 3D). Consistent with previous reports [6, 7], there were no CFU-F capable cells in the LepR/Tomato$^-$ BM stromal population (Fig. 3D). Contrary to our expectations, the CFU-F capacity of the LepR/Tomato$^+$/Runx2-GFP^{low} BM stromal population was high (Fig. 3D). CFU-F colonies derived from the LepR/Tomato$^+$/Runx2-GFP^{low} BM stromal population were positive for LepR/Tomato and weakly Runx2-GFP$^-$ positive (Fig. 3E,F). Furthermore, when BM stromal fractions were plated at clonal densities under nonadherent culture conditions, the LepR/Tomato$^+$/Runx2-GFP^{low} population formed spheres

(mesenspheres) at greater frequency than other fractions (Fig. 3G,H). The LepR/Tomato^{+}/Runx2-GFP^{low} BM stromal cells exhibited tri-lineage differentiation potential (Fig. 3I–K). However, it is not clear whether the LepR/Tomato^{+}/Runx2-GFP^{low} BM stromal cells generate other types of BM stromal cells. Real-time PCR analyses revealed that the LepR/Tomato^{-} sub-population did not express the MSPC markers *PDGFRα* [7, 33] *LepR* [5, 6] or *CXCL12* [23] (Fig. 3L-N). Interestingly, the expression levels of all three of these MSPC markers in the LepR-Cre/Tomato^{+}Runx2-GFP^{low} sub-population were significantly higher than in the LepR-Cre/Tomato^{+}Runx2-GFP^{-} sub-population (Fig. 3L-N). These results also indicated that the LepR-Cre/ Tomato^{+}Runx2-GFP^{low} sub-population overlaps with CXCL12 abundant reticular (CAR) cells [23], which are generated from part of the developing chondrogenic cell populations [17]. The expression levels of *Runx2* mRNA in the Runx2-GFP^{low} sub-population were significantly higher than those in the Runx2-GFP^{-} sub-population from LepR-Cre/Tomato^{+} stromal cells (Fig. 3O). The *Runx2* expression was hardly detected in the LepR-Cre/Tomato^{-} stromal cell population at the mRNA level (Fig. 3O). Consistently, the LepR-Cre/Tomato^{-} stromal population contained almost no Runx2-GFP^{+} cells (0.7 ± 0.2%) (Fig. 4). Taken together, these results indicate that stromal stem cell activity in BM is high in LepR^{+}Runx2-GFP^{low} stromal cell populations. Therefore, our findings provide evidence that LepR^{+} Runx2-GFP^{low} cells sit atop the BM stromal cell hierarchy, and the osteoblastic master transcription factor Runx2 is weakly expressed in BM-MSPC populations without osteoblastic lineage commitment.

4.3 LepR^{+}Runx2-GFP^{low} cells differentiate into osteoblasts through multilayered cell formation in response to PTH anabolic effects.

In vivo genetic lineage tracing analysis demonstrated that LepR^{+} cells differentiate into osteoblasts [5, 6]. As we found that stem cell activity is enriched in LepR^{+}Runx2-GFP^{low} BM stromal cell populations, we next examined whether LepR^{+}Runx2-GFP^{low} cells differentiate into mature osteoblasts *in vivo* by lineage tracing. Because intermittent treatment of parathyroid hormone (PTH) (1–34) increased bone volume by inducing bone formation (Fig. 5) [24–26, 28], we injected PTH into LepR/Tomato/Runx2-GFP mice. Bone-lining osteoblasts were detected as Runx2-GFP single-positive cells in the control group (Fig. 6A, asterisks). In contrast,

LepR/Tomato and Runx2-GFP double-positive mature osteoblasts were significantly increased on the endosteal surface in the PTH-treated bone tissue (Fig. 6B, asterisks and Fig. 7A). These results suggest that osteoblastogenesis from LepR^{+} cells is accelerated by PTH treatment. It is noteworthy that while LepR^{+}Runx2-GFP^{low} cells were observed in the control BM cavity (Fig. 6A and Fig. 8A, arrows), LepR^{+}Runx2-GFP^{+} multilayered cells (designated as ML-cells) were observed in the vicinity of bone tissue by PTH treatment (Fig. 6B and Fig. 8B, arrows). Quantification of vertical- and cross-section images revealed that ML-cells were significantly increased by PTH treatment (Fig. 7B and 8C–E). The expression level of Runx2-GFP in ML-cells was higher than in LepR^{+}Runx2-GFP^{low} cells (Fig. 6A, B, right panels, arrows). In contrast, the expression level of Runx2-GFP in ML-cells was lower than in cuboidal-shaped osteoblasts (Fig. 6B, right panel, arrows and asterisks). These results suggest that the LepR^{+}Runx2-GFP^{low} cells differentiate into mature osteoblasts through ML-cell formation with increasing levels of Runx2 expression.

4.4 LepR^{+}Runx2-GFP^{low} cell-derived multilayered cells differentiate into mature osteoblasts with increasing expression of Osterix and type I collagen α.

We next analyzed the expression pattern of Osterix (Osx), a transcription factor downstream of Runx2, in ML-cells using Osx-Cre^{ERT2}(iOsx)/Tomato/Runx2-GFP mice, administering tamoxifen for labeling of Osx^{+} cells [34]. Histological analyses demonstrated that mature osteoblasts express both iOsx/Tomato and Runx2-GFP, but Runx2-GFP^{low} cells located away from bone surfaces were negative for iOsx/Tomato (Fig. 6C, asterisks and arrowheads). ML-cells located far from osteoblasts were iOsx/Tomato negative, but those near bone-lining osteoblasts were positive for Tomato (Fig. 6D, arrowheads and arrows). Both the iOsx/Tomato-negative and -positive ML-cells (Runx2-GFP^{+} cells) were significantly increased by the PTH treatment (Fig. 7C and D).

Lastly, we examined the hierarchical relationship between Osx and Type- I collagen α (Col1), a marker for mature osteoblasts, in osteoblastogenesis from ML-cells using iOsx/Tomato/ Col1(2.3)-GFP mice. Tamoxifen-induced iOsx/Tomato^{+} cells were observed as mature osteoblasts with Col1(2.3)-GFP expression in control bone

tissue (Fig. 6E, asterisks). However, iOsx/Tomato^{+} cells were observed as ML-cells after PTH-treatment (Fig. 6F). Only the population of these cells localized in the vicinity of the bone surface overlapped with Col1(2.3)-GFP expression (Fig. 6F, compare arrowheads and arrows). Both the Col1(2.3)-GFP-negative and-positive ML-cells (iOsx/Tomato^{+} cells) were significantly increased by the PTH treatment (Fig. 7E and F).These results thus suggest that LepR^{+}Runx2-GFP^{low} cells differentiate into ML-cells adjacent to the bone surface, and that PTH treatment enhances Runx2 expression, which subsequently induces Osx expression, resulting in differentiation into Col1^{+} mature osteoblasts (Fig. 9).

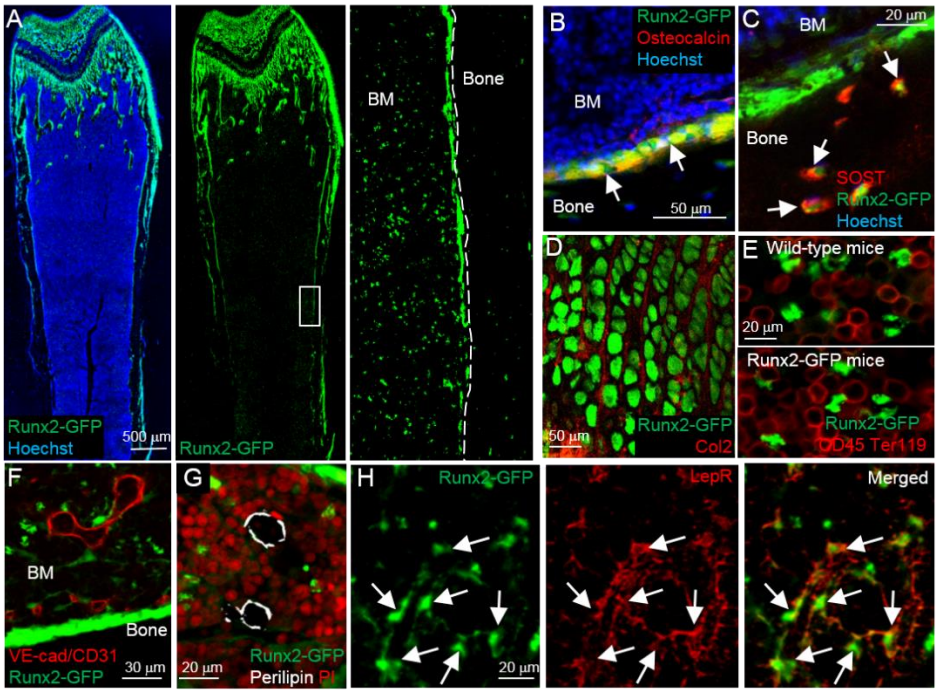

Figure 1. LepR$^+$ cells in the bone marrow cavity express Runx2.

(A–H) Z-stack confocal (A,D–F and H) and confocal (B,C and G) images of thick bone sections of Runx2-GFP mice (5–6 weeks old). The images were taken from whole bone tissue (A), endosteum (B,C and F), epiphyseal cartilage (D) and bone marrow (E,G and H). Bone tissues are stained with osteocalcin (Red) (B), SOST (Red) (C), Type-2 collagen (Col2) (Red) (D), CD45 and Ter119 (Red) (E), VE-cadherin (VE-Cad) and CD31 (Red) (F), Perilipin (White) (G), and Leptin receptor (LepR) (Red) (H) antibodies. Nuclei are visualized with Hoechst 33342 (blue) and propidium iodide (PI) (Red). Arrows: Osteoblasts (B), Osteocytes (C), and LepR$^+$ cells (H).

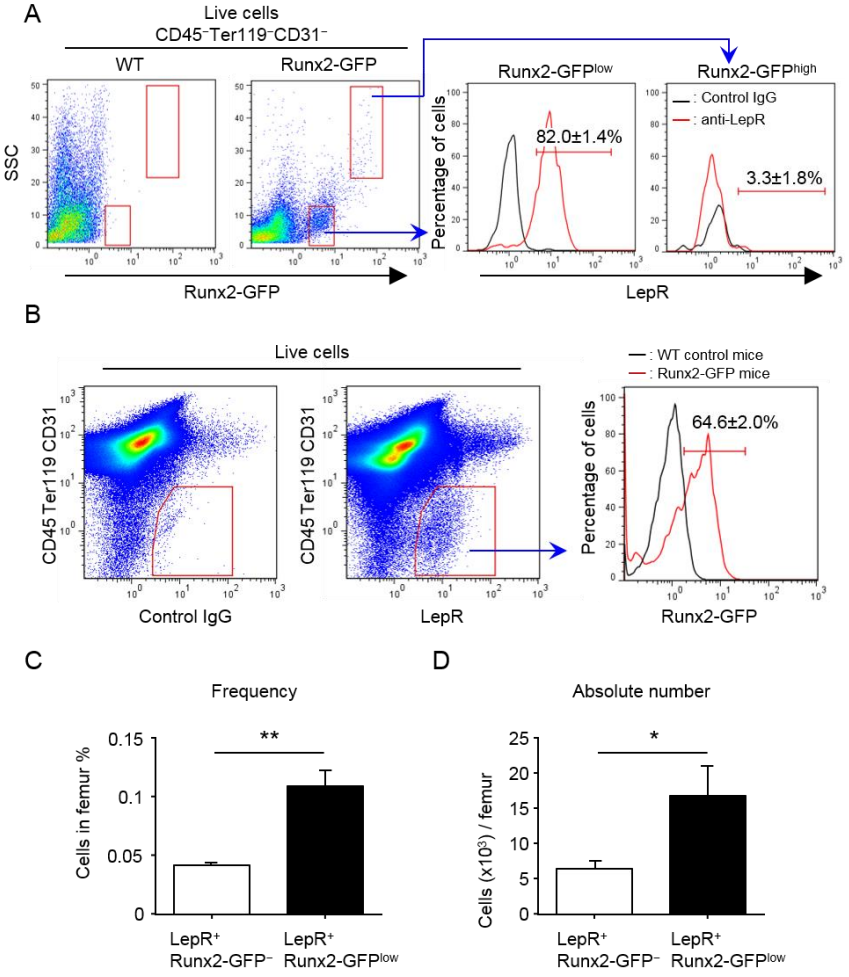

Figure 2. LepR$^+$ cells contain Runx2-GFP^{low} and Runx2-GFP$^-$ sub-populations.

(A) Representative FACS plots (gated on live CD45$^-$Ter119$^-$CD31$^-$ cells) showing the expression of LepR in Runx2-GFP$^+$ stromal populations from 5 week-old Runx2-GFP mice. Left panel showing representative FACS plot of WT control (gated on live CD45$^-$Ter119$^-$CD31$^-$ cells). Black and red lines represent the isotype control and specific antibody against LepR, respectively. n = 3. (B) Representative FACS plots (gated on live cells) showing frequency of Runx2-GFP$^+$ population in the CD45$^-$Ter119$^-$CD31$^-$LepR$^+$ cell population (right panel) from 5–6 week-old Runx2-GFP mice. Left panel showing negative control for LepR antibody (gated on live cells). Black and red lines represent the WT control and Runx2-GFP mice, respectively (right panel). n = 3. (C and D) Quantification of the frequency (C) and absolute number (D) of Runx2-GFP^{low} and Runx2-GFP$^-$ sub-populations in LepR$^+$ cells (CD45$^-$Ter119$^-$CD31$^-$). n = 3. *$p < 0.05$, **$p < 0.01$. Data are represented as mean ± SD.

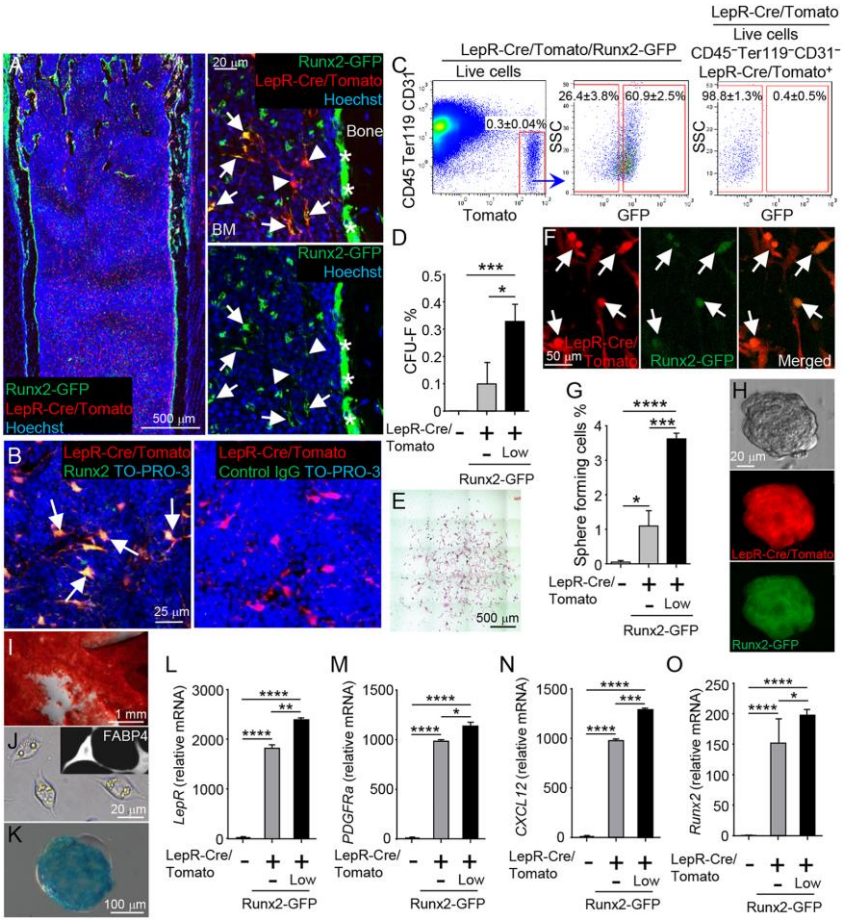

Figure 3. Stromal stem cell activity in BM is enriched in LepR$^+$Runx2-GFP^{low} population.

(A) Z-stack confocal images of thick bone sections of 6 week-old LepR-Cre/Tomato/Runx2-GFP mice. Arrows: LepR-Cre-derived Tomato$^+$ (LepR/Tomato$^+$)/Runx2-GFP^{low} cells. Arrowheads: LepR/Tomato$^+$/ Runx2-GFP$^-$ cells. *: Runx2-GFP^{high} bone-lining mature osteoblasts. Nuclei were visualized with Hoechst 33342 (blue). (B) Z-stack confocal images of thick bone sections of 6 week-old LepR-Cre/Tomato mice stained with Runx2 (left panel, green) and control IgG (right panel). Arrows: LepR/Tomato$^+$/Runx2$^+$cells. Nuclei are visualized with To-PRO-3 (blue). (C) Representative FACS plots (gated on live cells) showing the percentages of Runx2-GFP-positive (designated as Runx2-GFP^{low}) and -negative (designated as Runx2-GFP$^-$)cells (middle panel) in the CD45$^-$Ter119$^-$CD31$^-$LepR/Tomato$^+$ stromal population (left panel) from 6 week-old LepR-Cre/Tomato/Runx2-GFP mice. Right panel showing representative FACS plot of control (gated on live D45$^-$Ter119$^-$CD31$^-$LepR/Tomato$^+$ cells) in 6 week-old LepR-Cre/Tomato mice. (D–O) CD45$^-$Ter119$^-$CD31$^-$ stromal cells (gated on live cells) were sorted based on expression of LepR-Cre/Tomato and Runx2-GFP from 6–7 week-old LepR-Cre/Tomato/Runx2-GFP mice, and percentage of CFU-F (D) and clonal sphere (mesensphere) formation (G) were determined. Representative image of CFU-F colony (E; Giemsa staining, F; Tomato and GFP fluorescence). n = 3 independent experiments. Arrows: LepR/Tomato and Runx2-GFP double-positive cells. Representative image of mesensphere formation (H; bright field, Tomato, and GFP fluorescence). n = 3 independent experiments. Differentiation phenotypes of LepR/Tomato$^+$/Runx2-GFP^{low} cells shown by Alizarin Red S: osteoblasts (I), lipid droplets and staining with FABP4 antibody: adipocytes (J), and Alcian Blue: chondrocytes (K). Expression levels of *LepR* (L), *PDGFRa* (M), *CXCL12* (N) and *Runx2* (O) were measured by quantitative real-time PCR. n = 3–5. *$p < 0.05$, **$p < 0.01$, ***$p < 0.001$, ****$p < 0.0001$. Data are represented as mean ± SD.

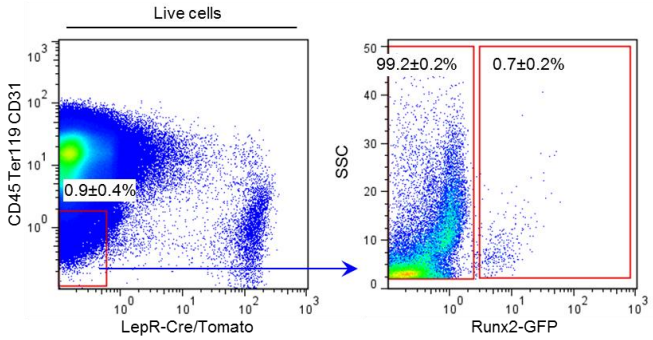

Figure 4. Runx2-GFP^{+} cells are hardly detected in the CD45^{-}Ter119^{-}CD31^{-}LepR/Tomato^{-} stromal population

Representative FACS plots (gated on live cells) showing the percentages for Runx2-GFP-positive and -negative cells (right panel) in the CD45^{-}Ter119^{-}CD31^{-}LepR/Tomato^{-} stromal population (left panel) from 6 week-old LepR-Cre/Tomato/Runx2-GFP mice.

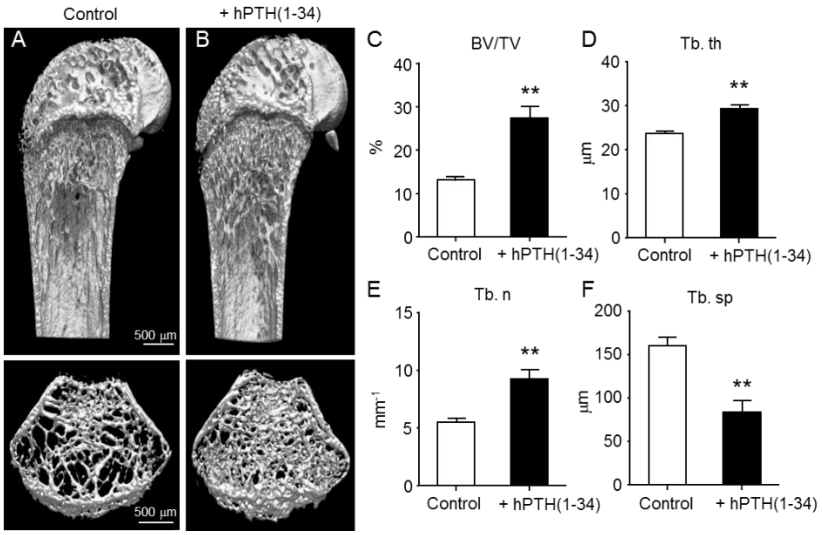

Figure 5. Intermittent PTH treatment increases bone mass of wild-type mice.

Six week-old wild-type mice were treated with vehicle and hPTH(1–34). Representative micro-CT images (A and B) and quantification of bone parameters (C-F). BV/TV, trabecular bone volume/total volume ratio (C), Tb. th., trabecular thickness (D); Tb. n., trabecular number (E); Tb. sp., trabecular separation (F). n=6. **p < 0.01*. Data are represented as mean ± SD.

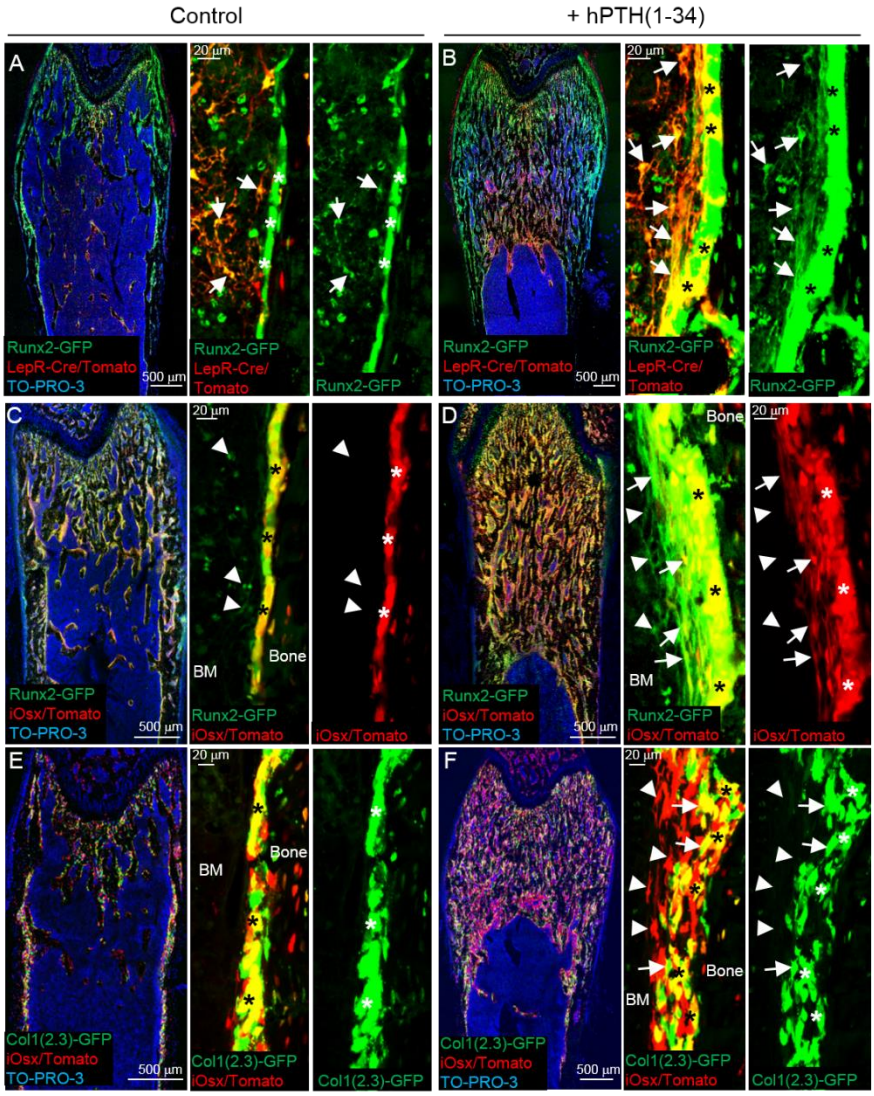

Figure 6. LepR^{+}Runx2-GFP^{low} cells differentiate into osteoblasts through multilayered cell formation in response to PTH-induced anabolic effects.

(A–F) Z-stack confocal images of thick bone sections of 6 week-old LepR-Cre/Tomato/Runx2-GFP mice (A and B), tamoxifen-administered iOsx/Tomato/Runx2-GFP mice (C and D), and tamoxifen-administered iOsx/Tomato/Col1(2.3)-GFP mice (E and F) with vehicle (A,C and E) and hPTH(1–34) (B,D and F) intermittent treatment. Arrows: LepR-Cre-derived Tomato^{+}(LepR/Tomato^{+}) Runx2-GFP^{+} cells (A and B), iOsx/Tomato^{+}Runx2-GFP^{+} cells (D) and iOsx/Tomato^{+}Col1(2.3)-GFP^{+} cells (F). Arrowheads: iOsx/Tomato^{-}Runx2-GFP^{+} cells (C and D) and iOsx/Tomato^{+}Col1(2.3)-GFP^{-} cells (F). *: Bone lining mature osteoblasts. Nuclei were visualized with To-PRO-3 (blue).

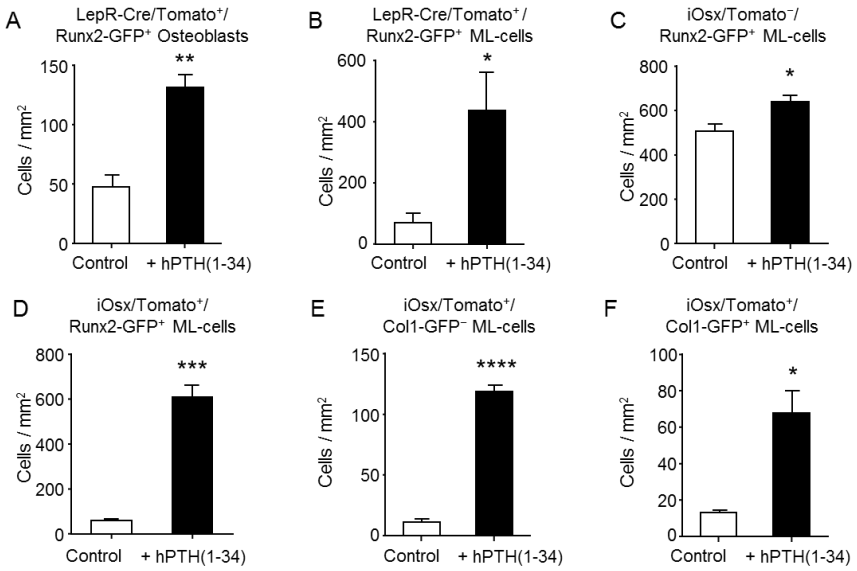

Figure 7. Osteoblastogenesis and multilayered (ML)-cells are induced in response to intermittent PTH treatment.

Six week-old LepR-Cre/Tomato/Runx2-GFP mice (A and B), tamoxifen-administered iOsx/Tomato/Runx2-GFP mice (C and D) and tamoxifen-administered iOsx/Tomato/Col1(2.3)-GFP mice (E and F) with vehicle and hPTH(1-34) intermittent treatment. Quantification of LepR-Cre/Tomato$^+$/Runx2-GFP$^+$ osteoblasts (A), LepR/Tomato$^+$/Runx2-GFP$^+$ ML-cells (B), iOsx/Tomato$^-$ Runx2-GFP$^+$ ML-cells, (C), iOsx/Tomato$^+$Runx2-GFP$^+$ ML-cells (D), iOsx/Tomato$^+$Col1(2.3)-GFP$^-$ ML-cells (E) and iOsx/Tomato$^+$Col1(2.3)-GFP$^+$ ML-cells (F) in 1 mm^2 within 200 μm from the bone surface. n=3-6 sections. *$p < 0.05$, **$p < 0.01$, ***$p < 0.001$, ****$p < 0.0001$. Data are represented as mean ± SD.

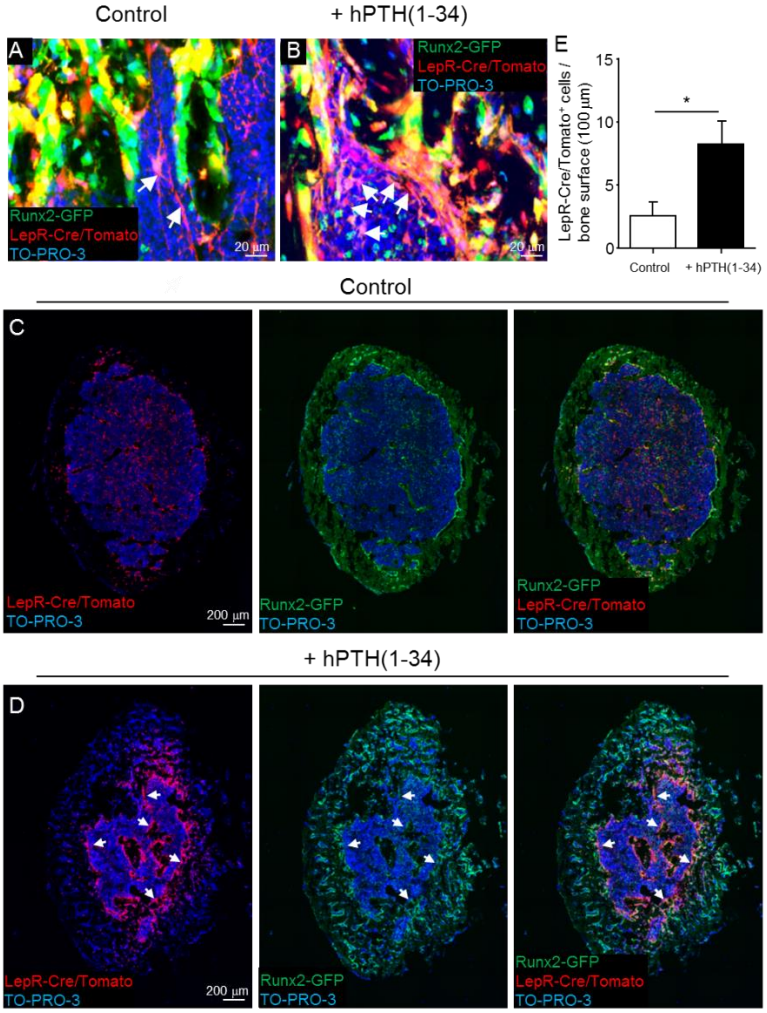

Figure 8. Multilayered (ML)-cells are formed along the bone surface in response to intermittent PTH treatment.

(A-D) Z-stack confocal images of thick bone sections of 6 week-old LepR-Cre/Tomato/Runx2-GFP mice with vehicle (A and C) and hPTH (1-34) (B and D) intermittent treatment. Arrows: LepR-Cre-derived Tomato$^+$(LepR/Tomato$^+$)Runx2-GFP$^+$ cells (A, B and D). (E) Quantification of the number of LepR/Tomato$^+$ ML-cells within 50 μm from the bone surface. n=3. $*p < 0.05$. Data are represented as mean ± SD. Nuclei were visualized with To-PRO-3 (blue).

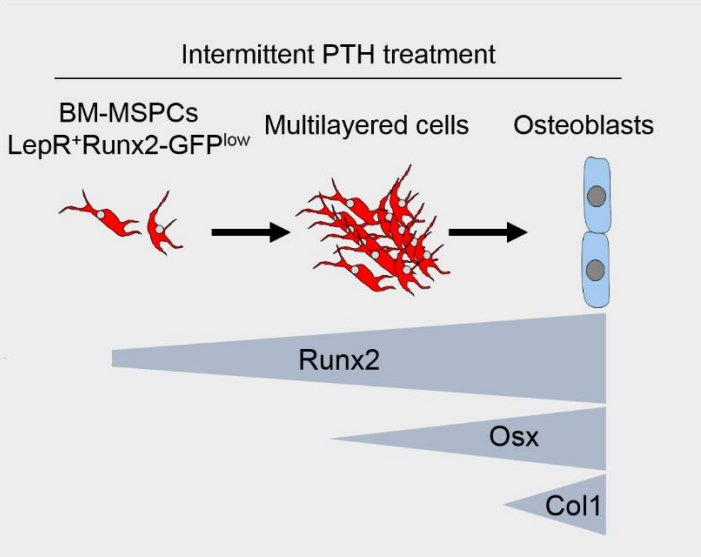

Figure 9. Differentiation model of LepR^{+}Runx2-GFP^{low} cells into osteoblasts.

LepR^{+}Runx2-GFP^{low} cells form multilayered structures along the bone surface in response to intermittent PTH treatment. In this process, the LepR^{+}Ranx2-GFP^{low} cells increase the expression levels of Runx2, Osx and Col1 sequentially, and eventually differentiate into mature osteoblasts.

5. DISCUSSION

To clarify *in vivo* osteoblastogenesis from LepR$^+$ cells, we analyzed the expression pattern of the early osteoblastic transcription factor, Runx2, in LepR$^+$ cells using Runx2-GFP transgenic mice [31]. Here we report that BM-MSPCs in adult BM are confined to the weak Runx2-GFP-expressing LepR$^+$ stromal cell population, which differentiates into Col1$^+$ mature osteoblasts in response to PTH anabolic effects. In this process, the LepR$^+$Runx2-GFP^{low} cells form multilayered structures along the bone surface, subsequently increasing expression levels of Runx2 and Osx.

Our results demonstrating that the stem cell capacity is enriched in Runx2-GFP^{low} populations are consistent with recently published data in which the most primitive stromal population in the calvaria, gated as Prx1$^+$Scal$^+$cells, expresses Runx2 at low levels [35]. On the other hand, a single-cell assay demonstrated that CXCL12 abundant reticular (CAR) cells, which largely overlap with the LepR$^+$ cell population, express not only Runx2 and Osx, but also peroxisome proliferator-activated receptor γ (PPAR γ), an essential transcription factor for adipogenesis [36], at the mRNA level [23]. Interestingly, osteoblastogenesis is enhanced by decreased transcriptional activity and haploinsufficiency of PPAR γ in BM stromal progenitors [37, 38]. In contrast, adipogenesis is accelerated due to the stromal deletion of Wnt/β-catenin-signaling, an essential signaling pathway for osteoblastogenesis [39]. These reports suggest that the undifferentiated state of LepR$^+$Runx2-GFP^{low} cells is sustained due to reciprocal inhibition between osteogenic and adipogenic factors. Several studies have reported that the lineage differentiation of BM-MSPCs is skewed toward osteoblasts by intercellular expression of vascular endothelial growth factor A (VEGF-A) [40]. In contrast, the adipocyte lineage commitment from BM-MSPCs is increased by up-regulation of MicroRNA-188 [41], deletion of transcription factor Foxc [9] and peripheral Leptin/Leptin receptor signaling [10]. Further studies will clarify the mechanistic details of the cell fate decision of BM-MSPCs.

Our data demonstrate that CFU-F and mesensphere forming capacities are rarely observed in the Runx2-GFP$^-$stromal sub-population of LepR$^+$ cells. These

results indicate that the LepR$^+$Runx2-GFP$^-$ stromal sub-population contains some kind of committed cells other than stem cells. Previous studies provide *in vivo* evidence demonstrating that LepR$^+$ cells differentiate into not only osteoblasts but also adipocytes with aging and during tissue regeneration processes after injury [5, 6]. In the process of adipogenesis, the expression levels of Runx2 decrease, as opposed to the increase of PPARγ [40]. Furthermore, our immunofluorescence data demonstrated that adipocytes are negative for Runx2 (Fig. 1G). These data suggest that the LepR$^+$Runx2-GFP$^-$ stromal sub-population may be adipocyte-committed precursors. Further analysis of this fraction will provide information about the process of adipocytogenesis from BM-MSPCs *in vivo*.

In this study, we demonstrated that the PTH treatment accelerated osteoblastogenesis from LepR$^+$Runx2-GFP^{low} cells. It has been shown that mature osteoblasts are continuously replaced by immature precursors in adult bone tissues [42]. Because the LepR$^+$ cells differentiate into osteoblasts in adult bone tissues [5, 6], the LepR$^+$Runx2-GFP^{low} cells contribute to bone remodeling and maintain bone homeostasis in the adult phase. On the other hand, it has been reported that PTH anabolic effects are exerted by activation of quiescent bone lining osteoblasts [43], suggesting that the PTH has multiple targets for bone anabolism. Our results also demonstrate that ML-cells appear along the bone surface by PTH treatment. Consistent with our results, it is reported that clustered Osx-positive cells are observed as pre-osteoblasts in the vicinity of trabecular bone surfaces from PTH-treated rats [27]. Others, by employing proliferating cell labeling experiments, have also reported that the PTH-induced thick layered cells proliferate with expression of osteoblastic markers such as alkaline phosphatase (ALP), Runx2, osteocalcin and osteonectin [29, 30]. These results indicate that the PTH-induced osteoblastic differentiation is associated with cell cycle progression. Previous studies reported that the LepR$^+$ cells are quiescent in adult BM [5, 6]. However, the LepR$^+$ cells markedly proliferate in response to self-depletion, and lineage differentiation into both osteoblasts and adipocytes is accelerated concomitantly in this situation [6]. In contrast, depletion of the transcription factors Snail and Slug in the skeletal stem cells decreases not only proliferative activity but also lineage commitment potential, coincidently [44]. These results suggest that cell cycle quiescence may be critical for

maintaining the undifferentiated state of BM-MSPCs. Further analysis of the mechanistic relationship between cell cycle regulation and lineage commitment of $LepR^{+}Runx2\text{-}GFP^{low}$ cells will provide a potential therapeutic target for osteoporotic patients.

6. REFERENCES

1. Bianco P, Cao X, Frenette PS, Mao JJ, Robey PG, Simmons PJ, Wang CY (2013) The meaning, the sense and the significance: translating the science of mesenchymal stem cells into medicine. *NatMed* 19 : 35–42.
2. Frenette PS, Pinho S, Lucas D and Scheiermann C (2013) Mesenchymal stem cell: keystone of the hematopoietic stem cell niche and a stepping-stone for regenerative medicine. *Annu Rev Immunol* 31 : 285–316.
3. Kfoury Y and Scadden DT (2015) Mesenchymal cell contributions to the stem cell niche. *Cell Stem Cell* 16 : 239–253.
4. Ding L, Saunders TL, Enikolopov G and Morrison SJ (2012) Endothelial and perivascular cells maintain haematopoietic stem cells. *Nature* 481 : 457–462.
5. Mizoguchi T, Pinho S, Ahmed J, Kunisaki Y, Hanoun M, Mendelson A, Ono N, Kronenberg HM, Frenette PS (2014) Osterix marks distinct waves of primitive and definitive stromal progenitors during bone marrow development. *Dev Cell* 29 : 340–349.
6. Zhou BO, Yue R, Murphy MM, Peyer JG and Morrison SJ (2014) Leptin-receptor-expressing mesenchymal stromal cells represent the main source of bone formed by adult bone marrow. *Cell Stem Cell* 15 : 154–168.
7. Pinho S, Lacombe J, Hanoun M, Mizoguchi T, Bruns I, Kunisaki Y, Frenette PS (2013) PDGFRα and CD51 mark human nestin+ sphere-forming mesenchymal stem cells capable of hematopoieticprogenitor cell expansion. *J Exp Med* 210 : 1351–1367.
8. Ding L and Morrison SJ (2013) Haematopoietic stem cells and early lymphoid progenitors occupy distinct bone marrow niches. *Nature* 495 : 231–235.
9. Omatsu Y, Seike M, Sugiyama T, Kume T and Nagasawa T (2014) Foxc1 is a critical regulator of haematopoietic stem/progenitor cellniche formation. *Nature* 508 : 536–540.
10. Yue R, Zhou BO, Shimada IS, Zhao Z and Morrison SJ (2016) Leptin receptor promotes adipogenesis and reduces osteogenesis by regulating mesenchymal stromal cells in adult bone marrow. *Cell Stem Cell* 18 : 782–796.
11. Greenbaum A, Hsu YM, Day RB, Schuettpelz LG, Christopher MJ, Borgerding

JN, Nagasawa T, Link DC (2013) CXCL12 in early mesenchymal progenitors is required for haematopoietic stem-cell maintenance. *Nature* 495 : 227–230.

12. Ducy P, Zhang R, Geoffroy V, Ridall AL and Karsenty G (1997) Osf2/Cbfa1: a transcriptional activator of osteoblast differentiation. *Cell* 89 : 747–754.
13. Komori T, Yagi H, Nomura S, Yamaguchi A, Sasaki K, Deguchi K, Shimizu Y, Bronson RT, Gao YH, Inada M, Sato M, Okamoto R, Kitamura Y, Yoshiki S, Kishimoto T (1997) Targeted disruption of Cbfa1 results in a complete lack of bone formation owing to maturational arrest of osteoblasts. *Cell* 89 : 755–764.
14. Otto F, Thornell AP, Crompton T, Denzel A, Gilmour KC, Rosewell IR, Stamp GW, Beddington RS, Mundlos S, Olsen BR, Selby PB, Owen MJ (1997) Cbfa1, a candidate gene for cleidocranial dysplasia syndrome, is essential for osteoblast differentiation and bone development. *Cell* 89, 765–771.
15. Adhami MD, Rashid H, Chen H, Clarke JC, Yang Y, Javed A (2015) Loss of Runx2 in committed osteoblasts impairs postnatal skeletogenesis. *J Bone Miner Res* 30 : 71–82.
16. Takarada T, Hinoi E, Nakazato R, Ochi H, Xu C, Tsuchikane A, Takeda S, Karsenty G, Abe T, Kiyonari H, Yoneda Y (2013) An analysis of skeletal development in osteoblast-specific and chondrocyte-specific runt-related transcriptionfactor-2 (Runx2) knockout mice. *J Bone Miner Res* 28 : 2064–2069.
17. Ono N, Ono W, Nagasawa T and Kronenberg HM (2014) A subset of chondrogenic cells provides early mesenchymal progenitors in growing bones. *Nat Cell Biol* 16 : 1157–1167.
18. Liu W, Toyosawa S, Furuichi T, Kanatani N, Yoshida C, Liu Y, Himeno M, Narai S, Yamaguchi A, Komori T (2001) Overexpression of Cbfa1 in osteoblasts inhibits osteoblast maturation and causes osteopenia with multiple fractures. *J Cell Biol* 155 : 157–166.
19. Maruyama Z, Yoshida CA, Furuichi T, Amizuka N, Ito M, Fukuyama R, Miyazaki T, Kitaura H, Nakamura K, Fujita T, Kanatani N, Moriishi T, Yamana K, Liu W, Kawaguchi H, Nakamura K, Komori T (2007) Runx2 determines bone maturity and turnover rate in postnatal bone development and is involved in bone loss in estrogen deficiency. *Dev Dyn* 236 : 1876–1890.
20. Nakashima K, Zhou X, Kunkel G, Zhang Z, Deng JM, Behringer RR, de Crombrugghe B (2002) The novel zinc finger-containing transcription factor

osterix is required for osteoblast differentiation and bone formation. *Cell* 108 : 17–29.

21. Baek WY, de Crombrugghe B and Kim JE (2010) Postnatally induced inactivation of Osterix in osteoblasts results in the reduction of bone formation and maintenance. *Bone* 46 : 920–928.
22. Liu Y, Strecker S, Wang L, Kronenberg MS, Wang W, Rowe DW, Maye P (2013) Osterix-cre labeled progenitor cells contribute to the formation and maintenance of the bone marrow stroma. *PLoS One* 8(8) : e71318.
23. Omatsu Y, Sugiyama T, Kohara H, Kondoh G, Fujii N, Kohno K, Nagasawa T (2010) The essential functions of adipo-osteogenic progenitors as the hematopoietic stem and progenitor cell niche. *Immunity* 33 : 387–399.
24. Neer RM, Arnaud CD, Zanchetta JR, Prince R, Gaich GA, Reginster JY, Hodsman AB, Eriksen EF, Ish-Shalom S, Genant HK, Wang O, Mitlak BH (2001) Effect of parathyroid hormone (1-34) on fractures and bone mineral density in postmenopausal women with osteoporosis. *N Engl J Med* 344 : 1434–1441.
25. Alexander JM, Bab I, Fish S, Müller R, Uchiyama T, Gronowicz G, Nahounou M, Zhao Q, White DW, Chorev M, Gazit D, Rosenblatt M (2001) Human parathyroid hormone 1-34 reverses bone loss in ovariectomized mice. *J Bone Miner Res* 16 : 1665–1673.
26. Jilka RL (2007) Molecular and cellular mechanisms of the anabolic effect of intermittent PTH. *Bone* 40 : 1434–1446.
27. Ogura K, Iimura T, Makino Y, Sugie-Oya A, Takakura A, Takao-Kawabata R, Ishizuya T, Moriyama K, Yamaguchi A (2016) Short-term intermittent administration of parathyroid hormone facilitates osteogenesis by different mechanisms in cancellous and cortical bone. *Bone Rep* 5 : 7-14.
28. Yamamoto T, Hasegawa T, Sasaki M, Hongo H, Tsuboi K, Shimizu T, Ota M, Haraguchi M, Takahata M, Oda K, Luiz de Freitas PH, Takakura A, Takao-Kawabata R, Isogai Y, Amizuka N. (2016) Frequency of Teriparatide administration affects the aistological pattern of bone formation in young adult male mice. *Endocrinology* 157 : 2604–2620.
29. Lotinun S, Sibonga JD and Turner RT (2005) Evidence that the cells responsible for marrow fibrosis in a rat model for hyperparathyroidism are preosteoblasts. *Endocrinology* 146 : 4074–4081.

30. Luiz de Freitas PH, Li M, Ninomiya T, Nakamura M, Ubaidus S, Oda K, Udagawa N, Maeda T, Takagi R, Amizuka N (2009) Intermittent PTH administration stimulates pre-osteoblastic proliferation without leading to enhanced bone formation in osteoclast-less c-fos(-/-) mice. *J Bone Miner Res* 24 : 1586–1597.
31. Kawane T, Komori H, Liu W, Moriishi T, Miyazaki T, Mori M, Matsuo Y, Takada Y, Izumi S, Jiang Q, Nishimura R, Kawai Y, Komori T (2014) Dlx5 and mef2 regulate a novel runx2 enhancer for osteoblast-specific expression. *J Bone Miner Res* 29 : 1960–1969.
32. Komori, T. (2011) Signaling networks in RUNX2-dependent bone development. *J Cell Biochem* 112 : 750–755.
33. Morikawa S, Mabuchi Y, Kubota Y, Nagai Y, Niibe K, Hiratsu E, Suzuki S, Miyauchi-Hara C, Nagoshi N, Sunabori T, Shimmura S, Miyawaki A, Nakagawa T, Suda T, Okano H, Matsuzaki Y (2009) Prospective identification, isolation, and systemic transplantation of multipotent mesenchymal stem cells in murine bone marrow. *J Exp Med* 206 : 2483–2496.
34. Maes C, Kobayashi T, Selig MK, Torrekens S, Roth SI, Mackem S, Carmeliet G, Kronenberg HM. (2010) Osteoblast precursors, but not mature osteoblasts, move into developing and fractured bones along with invading blood vessels. *Dev Cell* 19 : 329–344.
35. Takarada T, Nakazato R, Tsuchikane A, Fujikawa K, Iezaki T, Yoneda Y, Hinoi E (2016) Genetic analysis of Runx2 function during intramembranous ossification. *Development* 143 : 211–218.
36. Barak Y, Nelson MC, Ong ES, Jones YZ, Ruiz-Lozano P, Chien KR, Koder A, Evans RM (1999) PPAR gamma is required for placental, cardiac, and adipose tissue development. *Mol Cell* 4 : 585–595.
37. Akune T, Ohba S, Kamekura S, Yamaguchi M, Chung UI, Kubota N, Terauchi Y, Harada Y, Azuma Y, Nakamura K, Kadowaki T, Kawaguchi H (2004) PPARgamma insufficiency enhances osteogenesis through osteoblast formation from bone marrow progenitors. *J Clin Invest* 113 : 846–855.
38. Cao Y, Gomes SA, Rangel EB, Paulino EC, Fonseca TL, Li J, Teixeira MB, Gouveia CH, Bianco AC, Kapiloff MS, Balkan W, Hare JM (2015) S-nitrosoglutathione reductase-dependent PPARγ denitrosylation participates in

MSC-derived adipogenesis and osteogenesis. *J Clin Invest* 125 : 1679–1691.

39. Song L, Liu M, Ono N, Bringhurst FR, Kronenberg HM, Guo J (2012) Loss of wnt/β-catenin signaling causes cell fate shift of preosteoblasts from osteoblasts to adipocytes. *J Bone Miner Res* 27 : 2344–2358.
40. Liu Y, Berendsen AD, Jia S, Lotinun S, Baron R, Ferrara N, Olsen BR (2012) Intracellular VEGF regulates the balance between osteoblast and adipocyte differentiation. *J Clin Invest* 122 : 3101–3113.
41. Li CJ, Cheng P, Liang MK, Chen YS, Lu Q, Wang JY, Xia ZY, Zhou HD, Cao X, Xie H, Liao EY, Luo XH (2015) MicroRNA-188 regulates age-related switch between osteoblast and adipocyte differentiation. *J Clin Invest* 125 : 1509–1522.
42. Park D, Spencer JA, Koh BI, Kobayashi T, Fujisaki J, Clemens TL, Lin CP, Kronenberg HM, Scadden DT (2012) Endogenous bone marrow MSCs are dynamic, fate-restricted participants in bone maintenance and regeneration. *Cell Stem Cell* 10 : 259–272.
43. Kim SW, Pajevic PD, Selig M, Barry KJ, Yang JY, Shin CS, Baek WY, Kim JE, Kronenberg HM (2012) Intermittent parathyroid hormone administration converts quiescent lining cells to active osteoblasts. *J Bone Miner Res* 27 : 2075–2084.
44. Tang Y, Feinberg T, Keller ET, Li XY and Weiss SJ (2016) Snail/Slug binding interactions with YAP/TAZ control skeletal stem cell self-renewal and differentiation. *Nat Cell Biol* 18 : 917–929.
45. Matsuo K, Kuroda Y, Nango N, Shimoda K, Kubota Y, Ema M, Bakiri L, Wagner EF, Takeda Y, Yashiro W, Momose A (2015) Osteogenic capillaries orchestrate growth plate-independent ossification of the malleus. *Development* 142 : 3912–3920.
46. Kawamoto T and Shimizu M (2000) A method for preparing 2- to 50-micron-thick fresh-frozen sections of large samples and undecalcified hard tissues. *Histochem Cell Biol* 113 : 331–339.
47. Mendez-Ferrer S, Michurina TV, Ferraro F, Mazloom AR, Macarthur BD, Lira SA, Scadden DT, Ma'ayan A, Enikolopov GN, Frenette PS (2010) Mesenchymal and haematopoietic stem cells form a unique bone marrow niche. *Nature* 466 : 829–834.

Chapter 2

1. ABSTRACT

Intermittent parathyroid hormone (iPTH) treatment induces bone anabolic effects, resulting in healing of osteoporotic bone loss. Genetic lineage tracing approaches revealed that iPTH treatment induced osteoblastic differentiation from bone marrow (BM) mesenchymal stem and progenitor cells (MSPCs), which are marked by leptin receptor (LepR)-Cre. Although these findings suggest that part of the PTH-induced bone anabolic action is exerted due to osteoblastic commitment from MSPCs, little is known about the mechanistic details of these process *in vivo*. Here, we show that LepR$^+$MSPCs differentiate into type I collagen (Col1)$^+$ mature osteoblasts in response to iPTH treatement. Along with the osteoblastogenesis, the number of Col1$^+$ mature osteoblasts was increased around the bone surface, although most of them resided as quiescent cells. On the other hand, the number of LepR-Cre-marked lineage was also increased in the vicinity of bone tissue, and the cell cycle was accelerated in these cells by iPTH treatment. The expression levels of osterix (Osx) and type-I collagen (Col1), markers for osteoblasts, were increased in LepR$^+$MSPCs population in response to iPTH treatment. In contrast, the expression levels of Cebpb, PPARγ, and Zfp467, markers for adipocytes, were decreased in this population. Consistent with these results, 5-fluorouracil-induced BM adipogenesis was inhibited by iPTH treatment. Then, the bone volume was significantly increased in this situation. iPTH treatment of ovariectomized rats exerted remedial action not only in osteoporotic bone tissue but also in expanded BM adipose tissue. These results indicated that iPTH treatment skews the lineage differentiation of LepR$^+$MSPCs cells toward osteoblasts from adipocytes. In this process, the LepR$^+$MSPCs proliferate and differentiate into mature osteoblasts through cell cycle withdrawal.

2. INTRODUCTION

Bone tissue appears to be silent organ, but in fact it is constantly resorbed by osteoclasts and replaced with newly formed bone tissue by osteoblasts. These process are called bone remodeling [1, 2]. There is evidence that the mature osteoblasts are replaced with newly formed osteoblasts within 60 days [3]. Therefore, it is generally believed that osteoblastic lineage cells are continuously provided by immature stromal population, hereafter termed bone marrow (BM) mesenchymal stem and progenitor cells (MSPCs), and this process is an indispensable event for the maintenance of bone tissue homeostasis. Recent genetic lineage tracing approaches revealed that Leptin receptor (LepR)-Cre marks MSPCs, which are localized adjacent to the blood vessels in the whole BM cavity [4, 5]. $LepR^{+}$MSPCs differentiate into osteoblasts and adipocytes, and they also contribute to chondrocytes, which are formed in bone fractured callus. There is evidence that LepR-Cre-labeled BM population is largely consistent with the $CD31^{-}Ter119^{-}CD45^{-}$Nestin(Nes)-$GFP^{low}$ population [4, 6, 7], CAR [CXC chemokine ligand (CXCL)12-abundant reticular] cells [8, 9], and Prx1-Cre labeled population [10]. However, recent studies suggested that osteoblasts in the developmental stage are derived not from $LepR^{+}$MSPCs but from Gli1- or Sox9-labeled population, which are localized in metaphyseal BM [11, 12]. These populations provide $LepR^{+}$MSPCs in developing BM as well. Although the $Gli1^{+}$ population is diminished in the adult stage, $LepR^{+}$MSPCs persist in the whole BM cavity and work as an origin of stromal lineage throughout life.

It is generally considered that cell cycle quiescence is an essential property for stem cell maintenance in each adult tissue [13-15]. In response to tissue turnover or regeneration of injured tissue, resident stem cells differentiate into descendant cells with cell cycle progression, which is suggested a critical event for lineage commitment. Consistent with this general view, recent studies indicated that BM-MSPCs are maintained in a quiescent state in the adult stage and differentiate into osteoblasts with proliferation in response to tissue injury [4, 5]. Similarly to this situation, several studies have found that progenitors of osteoblasts expanded along the bone surface in response to intermittent treatment of teriparatide, a bone

anabolic agent for osteoporotic patients, composed of amino acid 1–34 of human PTH[PTH(1–34)] [16-21]. Recent lineage tracing analyses demonstrated that part of the PTH anabolic effect is exerted by acceleration of osteoblastogenesis from MSPC populations, which are labeled by LepR-Cre or Sox9-CreER^{T2} [21,22]. These findings raised the intriguing possibility that iPTH treatment may induce entry to the cell cycle by MSPC populations from a quiescent state and expand the osteoblastic lineage in the process of their differentiation.

Adipocytes and osteoblasts are suggested to originate from the same immature stromal population, BM-MSPCs, marked by LepR-Cre. It is known that BM adipose tissue is increased with a concomitant in decrease bone volume in osteoporotic patients [23-25]. This observation suggests that the differentiation fate of BM-MSPCs in osteoporotic patients is skewed toward adipocytes from osteoblasts. However, although several master transcription factors for osteoblastic and adipocytic lineages have been identified, the mechanism of cell fate switching to each lineages remains to be elucidated. Previous *in vitro* culture studies demonstrated that osteoblastogenesis was enhanced but adipogenesis was decreased by activation of type I PTH/PTH-related peptide (PTHrP) receptor signaling pathway [26-28]. Consistent with these reports, increased adipose tissue was observed in PTHrP heterozygous mice, whose bone volume was significantly decreased compared with wild-type mice [29]. These phenotypes were also observed in a conditional knockout of type I PTH/PTHrP receptor in whole BM stromal populations, suggesting that PTH acts directly on the stromal population to regulate cell fate decisions [22, 30]. However, the effect of iPTH treatment on the variance of osteoblastic and adipocytic gene expression in BM-MSPC population has yet to be clarified.

Here we show that PTH-induced osteoblastogenesis is accompanied by cell cycle progression of BM-MSPCs, which are localized around bone tissue. In addition, our data revealed that osteoblastic and adipogenic gene expression are increased and decreased, respectably, in the BM-MSPC population in response to iPTH treatment. We also examined the effect of iPTH treatment on accelerated adipocytic differentiation using a cancer chemotherapy agent and ovariectomy to estimate the cell fate switching capacity. We observed that iPTH treatment dramatically reduced

adipose tissue in the both conditions.

3. EXPERIMENTAL PROCEDURES

3.1 Experimental Animals

C57BL/6 mice were perchased from Japan SLC. B6.129-Lepr*tm2(cre)Rck*/J (LepR-Cre) and B6.Cg-*Gt(ROSA)26Sortm14(CAG-tdTomato)Hze*/J mice were purchased from Jackson Laboratory (Bar Harbor, ME). Col1(2.3)-Gfp [31] mice and Nestin-Gfp [48,49] mice were kindly provided by K. Matsuo in Keio University and G. Enikolopov in stony brook university, respectively. Femail Fischer 344/DuCrlCrli rats were perchased from Charles River Japan. All animals were maintained in pathogen-free conditions in animal facilities certified by the Animal Care and Use Committees of Matsumoto Dental University or Asahi Kasei Pharma Corp., and animal protocols were approved by those committee. All animal studies were performed in accordance with the Guidelines of the Matsumoto Dental University or Asahi Kasei Pharma Corp. Animal Care Committee.

3.2 Antibodies and reagents

The primary antibodies used were anti-Perilipin (D1D8) (Cell Signaling Technology, Danvers, MA); APC-anti-CD45 (30-F11), APC-anti-Ter-119 (Ter119), APC-, PE- or FITC-anti-Ki67 (SolA15) (all from eBioscience, Waltham, MA); Alexa Fluor 647-anti-CD31/PECAM-1 (MEC13.3) (Biolegend, San Diego, CA); biotin-anti-LepR and biotin-normal goat IgG-control (all from R&D systems, Minneapolis, MN). The secondary antibodies used were PE-Streptavidin (Beckman Coulter Life Sciences, Brea, CA); Alexa Fluor 647 donkey anti-rabbit IgG (Invitrogen, Waltham, MA). Nuclei were stained with Hoechst 33342 (Sigma-Aldrich, St. Louis, MO), TO-PRO-3 iodide (642/661) (Molecular Probes, Waltham, MA), Propidium Iodide Solution (Biolegend) or SYTO 9 (485/498) (Invitrogen).

3.3 Microscopy imaging

Mice were perfused with 4% paraformaldehyde (PFA) for fixation. Femora were removed and further fixed with 4% PFA for 24 hours at 4℃, incubated in 10%, 20% and 30% sucrose each for over than 2 hours at 4℃ for cryoprotection and embedded in SCEM medium (SECTION-LAB, Hiroshima, Japan). Sections, 20-μm-thick, were prepared using Kawamoto's film method [50]. Z-stack confocal projection

images were obtained from 2-μm interval images of 20-μm thick sections. Fluorescence images were acquired using a laser-scanning confocal microscope (LSM510) equipped with Plan-Apochromat (20×/0.8), ZEN and Axiovision software (all from Carl Zeiss, Oberkochen, Germany). The left tibiae were removed from rats and dissected free of soft tissue, fixed in 70% ethanol, stained with Villanueva bone stain, dehydrated in a graded series of ethanol, defatted in acetone and embedded in polymethyl methacrylate (Wako, Osaka, Japan) without decalcification. Then, the samples were fixed on plastic slides and 20-μm-thick transverse sections were ground at a level 3 mm proximal to the tibiofibular junction from each tibia using a micro grinding system (MG-4000, Exakt Technologies, Oklahoma, OK). Bright-field images were acuiered using a Lica DM5500B (Leica, Wetzlar, Germany) equipped with a RETIGA 2000R FAST1394 color CCD camera (Q IMAGING, Surrey, BC) and Image-Pro Plus (Media Cybernetics, Rockville, MD). Bone area (Cortical area / Total area %) from rat tibiae was measured by using Osteoplan (Carl Zeiss). The area of BM adipose tissue (Adipose area / Total area %) from rat tibiae was mesured the middle square region (276 μm × 276 μm) of the BM cavity using by Vidas (Carl Zeiss).

3.4 PTH and 5-FU treatment

Three-week- to 18-month-old mice were injected intraperitoneally with Human PTH(1–34) (80 μg/kg/24 or 12 h) (Asahi Kasei Phama Co. Ltd., Tokyo, Japan) for 10 days. To induce adipocytogenesis *in vivo*, 5-FU (Sigma-Aldrich) (250 mg/kg) was injected intrave-niously into mice. PTH treatment was started at 30 min after 5-FU injection. Twenty-four hours after the final PTH injection, mice were sacrificed and used for analyses. Six-month-old rats were ovariectomized or sham-operated as reported previously [51], and bled for 6 month to establish osteoporosis. OVX rats were divided into three groups. The sham group and one of OVX groups were injected subcutaneously with saline as a vehicle. The remaining two OVX groupes were injected subcutaneously with PTH(1–34) [60 μg/kg/week] and [20 μg/kg × 3 times/week] for 6 month, respectively. Three days after the final PTH injection, rats were sacrificed and used for analyses.

3.5 EdU incorporation experiments

Mice were injected intraperitoneally with EdU (Molecular probes) (1 mg), and

sacrificed after 6 hours. EdU-positive cells were detected using Click-iT Plus EdU Alexa FluorTM 647 Imaging Kit (Molecular probes), in accordance with the manufacturer's recommendations.

3.6 Preparation of BM cell suspension

BM cells were flushed from tibiae and femora with HBSS (Gibco, Waltham, MA) containing 0.1% collagenase IV (Gibco), 0.2% Dispase (Gibco) and 20U/ml DNase (Worthington Biochemical, Lakewood, NJ) and digested for 30 min at 37°C. BM cells were washed with PBS and suspended with PBS containing 2% FBS, 1 mM EDTA. Before performing the cell sorting, the BM suspension were inqubated with anti-CD31, -CD45 and -Ter119 microbeads, and depleated hematopoietic and endotherial cells using MACS LD Column (all from Miltenyi Biotec, Bergisch Gladbach, Germany).

3.7 Cell sorting and flow cytometry

Cell sorting experiments were performed using an FACSAria III equipped with FACS Diva6.1.3 software (all from BD Biosciences, San Jose, CA). Flow cytometric analyses were carried out using a Cytomics FC 500 flow cytometer equipped with CXP software (all from Beckman Coulter Life Sciences). Dead cells and debris were excluded by FSC, SSC, DAPI (Dojindo, Kumamoto, Japan) and Fixable Viability Dy4 eFluor 780 (eBioscience) staining profiles. Data were analysed with FlowJo software (BD Biosciences).

3.8 RNA isolation and quantitative real-time PCR

Sorted cells were collected to α-MEM containing 10% FBS (all from Sigma-Aldrich). The cells were wash with PBS, and reverse transcription of mRNA and amplification of cDNA were performed by using CellAmpTM Whole Transcriptome Amplification Kit (Real Time) Ver.2 (TAKARA, Shiga, Japan). Quantitative real-time PCR was performed using Fast SYBR Green and Applied Biosystems StepOnePlus™ (all from Applied Biosystems, Waltham, MA). Gene expression data was normalized to *Gapdh*. The sequences of primers for each gene were as follows:

	Forward	Reverse
Gapdh	TGTGTCCGTCGTGGATCTGA	TTGCTGTTGAAGTCGCAGGAG
Col1a1	TCAGTGCAATTGTGTTGCTGAAAG	GATACCAAACTGGGCGT GCTG
Fabp4	TGGGAACCTGGAAGCTTGTCTC	GAATTC CACGCCCAGTTTGA

Pparg	GGAGCCTAAGTTTGAGTTTGCTGTG	TGC AGCAGGTTGTCTTGGATG
Sp7	AGGCCTTTGCCAGTGCCTA	GCCAG ATGGAAGCTGTGAAGA
Zfp467	TTCCCAGAA GCATCCTTACCTATC	CAAACAACCTTTATGGCCTGTTCA
Alpl	ACACCTTGACTGTGGTTACTGCTGA	CCTTGTAGCCAGGCCCGTTA
Bglap	AGCAGCTTGGCCCAGACCTA	TAGCGCCGGAGTCTGTTCACTAC
Cebpb	TGATGCAATCCGGATCAA	CACGTGTGTTGCGTCAGTC

3.9 Microcomputed tomography analysis

Femora were fixed in 70% ethanol at 4℃. Three-dimensional (3D) reconstructions of femora were taken using a composite X-ray analysis system (ScanXmate-A080; Comscan Tecno, Kanagawa, Japan). Bone morphometric analysis was performed with TRI/3D-Bon (Ratoc System Engineering Co., Tokyo, Japan). We measured the parameters of bone volume over total volume (BV/TV), trabecular thickness (Tb.Th.), trabecular number (Tb.N.), and trabecular separation (Tb.Sp.).

3.10 Statistics

Statistical analyses were performed using GraphPad Prism7 (GraphPad Software Inc., La Jolla, CA). The data were analysed by the D'Agostino-Pearson test ($n \geqq 8$) or the Shapiro-Wilk test ($n<8$) to evaluate normal distribution. To compare two groups, equality of the two variances was assessed using F-test. When the data sets met both the test requirements for distribution and variance, Student's test was used. When the data did not meet one of the test requirement, non-parametric, Mann-Whitney U test was used. To compare multiple groups, one-way ANOVA with Tukey's multiple comparisons test was performed. The results were expressed as mean ± SD. Experiments were performed three times and similar results were obtained. $p<0.05$ was considered statistically significant.

4. RESULTS

4.1 iPTH treatment induces differentiation of LepR$^+$MSPCs into mature osteoblasts.

Based on a genetic lineage tracing approach, it was demonstrated that iPTH treatment induces the differentiation of LepR$^+$MSPCs into early-stage osteoblasts positive for Runx2 transcription factor [21]. To clarify whether the maturation of osteoblastogenesis is accelerated in this situation, we generated LepR-Cre/ROSA26-loxP-stop-loxP-tdTomato(Tomato)/type I collagen α[Col1(2.3)]-GFP mice, in which LepR$^+$MSPC-derived Col1$^+$ mature osteoblasts can be detected as Tomato and GFP double-positive cells (yellow cells) [4, 31]. Corresponding with previous studies, trabecular bone volume was increased by iPTH treatment (80 μg/kg/day) for 10 days (Table 1) [20, 21, 32, 33]. Histological and fluorescence-activated cell sorting (FACS) analyses revealed that LepR$^+$MSPC-derived mature osteoblasts were significantly increased in response to iPTH treatment (Fig. 1A and Table 2). The osteoblast lineage commitment from LepR-Cre/Tomato$^+$ cells was further accelerated by increasing frequency of iPTH injection (80 μg/kg/12 hr for 10 days) (Fig. 1B and Table 3). These results indicated that iPTH treatment facilitated osteoblastic differentiation not only in early stage but also in late maturation.

4.2 LepR$^+$MSPCs proliferate in response to iPTH treatment and differentiate into mature osteoblasts through cell cycle withdrawal.

Next, we analyzed the effect of iPTH treatment on number of mature osteoblasts along the endosteal surface using Col1(2.3)-GFP mice. Histological analyses revealed that the iPTH treatment significantly increased the number of the Col1(2.3)-GFP$^+$ mature osteoblasts (Fig. 2A and Table 4). Of note, Ki67-positive proliferating mature osteoblasts were hardly observed in control bone tissue and were not increased by iPTH treatment (Fig. 2A and Table 5). Similarly, there was no significant difference in the number of 5-ethynyl-2'-deoxyuridine (EdU)-incorporated Col1(2.3)-GFP$^+$ mature osteoblasts between control and iPTH-treated mice (Fig. 2B and Table 6). In contrast, the number of Ki67- and EdU-negative mature osteoblasts were significantly increased in iPTH-treated group (Table 5,6). These results

suggestd that iPTH treatment increased the number of mature osteoblasts but did not accelerate their cell cycle progression.

Next, we determined the effect of iPTH treatment on proliferation of LepR$^+$MSPCs. Consistent with our previous report, iPTH treatment increased LepR-Cre/Tomato$^+$ cells in the vicinity of the bone tissue (Fig. 3) [21]. The number of Ki67-expressing LepR-Cre/Tomato$^+$ cells along the bone surface was significantly increased in the iPTH-treated group (Fig. 2C and Table 7). FACS analysis showed that the frequency of proliferating cells in the whole BM LepR-Cre/Tomato$^+$ population was significantly increased by iPTH treatment (Table 8). Altogether, these results indicated that, in response to iPTH treatment, the LepR$^+$MSPCs proliferated and differentiated into mature osteoblasts through cell cycle withdrawal.

4.3 Lineage differentiation of LepR$^+$MSPCs is skewed toward osteoblasts from adipocytes by iPTH treatment.

Because LepR$^+$MSPCs have the potential to differentiate into both osteoblasts and adipocytes [4, 5], we next analyzed the effect of iPTH treatment on the expression levels of both lineage markers in MSPCs. There is evidence that LepR$^+$ population largely overlaps with stromal Nestin(Nes)-GFP^{low} population [4, 6, 7], therefore, we sorted the Nes-GFP and LepR double-positive BM population from Nes-GFP mice with or without iPTH treatment. Real-time PCR experiments revealed that osteoblast markers Osterix (Osx)/SP7 and Col1 were significantly increased by iPTH treatment, although alkaline phosphatase (ALP) expression was significantly decreased (Table 9). In contrast, the levels of adipocytic markers, including peroxisome proliferator-activated receptor-γ (PPARγ), CCAAT enhancer-binding protein-β (Cebpβ), and zinc finger protein 467 (Zfp467), were significantly decreased in this situation (Table 10). However, in consistent to these other adipocytic markers, Fabp4 expression was dramatically increased by iPTH treatment (Table 10). These results indicated that the genetic profile of LepR$^+$MSPCs tended to be switched to an osteoblastic lineage from an adipocytic lineage by iPTH treatment.

4.4 iPTH treatment suppresses induced-adipocytic differentiation of LepR$^+$

MSPCs

Previous studies demonstrated that BM adipocytes were derived from LepR+MSPCs as well [4, 5, 10]. Because we found that several adipocytic markers were suppressed in LepR+MSPCs by PTH treatment, we next observed BM adipocytes in these conditions. Perilipin-positive adipocytes were significantly decreased by iPTH treatment (Fig. 4A and Table 11). It is known that BM adipocytic differentiation is induced by injection of 5-fuluorouracil (5-FU), which is used for cancer chemotherapy [34, 35]. 5-FU treatment dramatically induced adipocytic differentiation in BM in a time-dependent manner (Fig. 5), but 5-FU-induced adipogenesis was significantly inhibited by iPTH treatment (Fig. 4B and Table 12). Even in 5-FU-treated conditions, bone volume was increased in the iPTH-treated group (Table 13). These data suggested that iPTH treatment switched the differentiation of LepR+MSPCs toward osteoblasts, resulting in a reduction of 5-FU-induced adipogenesis.

BM adipose tissue was suggested to be increased in postmenopausal osteoporotic patients [24, 36]. To test whether iPTH treatment has the potential to restore osteoporosis-induced fatty BM tissue, we performed iPTH treatment on ovariectomized (OVX) rats. Six month-old OVX rats were bred for addition 6 months in order to induce the onset of osteoporosis before the start of iPTH treatment. The OVX operation significantly decreased the relative cortical area and simultaneously increased adipocytes in the BM cavity compared to sham controls (Table 14). Both iPTH dosing schedules [60 μg/kg/week or 20 mg/kg × 3 times/week, designated as iPTH (60) and iPTH (20 × 3), respectively] increased relative cortical area to the same level as the sham control (Table 14). The healing effect on bone tissue in iPTH (20 × 3) treatment was tended to be higher than that in iPTH (60) treatment (Table 14). As opposed to bone tissue, OVX-induced BM adipose tissue was significantly decreased by iPTH treatments with both iPTH (60) and iPTH (20 × 3) treatment (Table 15). Importantly, the healing effects on adipose tissue in iPTH (20 × 3) treatment also tended to be higher than that in iPTH (60) treatment (Table 15). These results suggested that the greater increase in PTH induced-osteoblastogenesis in MSPCs, the greater the decrease in adipogenesis.

Overall, our findings indicated that the iPTH treatment on osteoporotic

patients exerted remedial action not only in osteoporotic bone tissue but also in the adipose BM cavity, through lineage switching of BM-MSPCs into osteoblasts.

Table 1 Effect of PTH(1-34) treatment on the morphometric parameters of bone tissue

Parameters (units)	PTH(1-34) Mean±SD
BV/TV (%)	↑ **
Tb.Th. (μm)	↑ **
Tb.N. (mm^{-1})	↑ **
Tb.Sp. (μm)	↓ **

Five-week-old mice were treated with vehicle or iPTH(1-34) (80 μg/kg/24 h) for 10 days. Quantification of bone parameters: BV/TV, bone volume over total volume; Tb.Th., trabecular thickness; TbN., trabecular number; Tb.Sp., trabecular separation. n=6–7. *$^{**}p < 0.01$, $^{***}p < 0.001$.* Data are shown as mean ± SD.

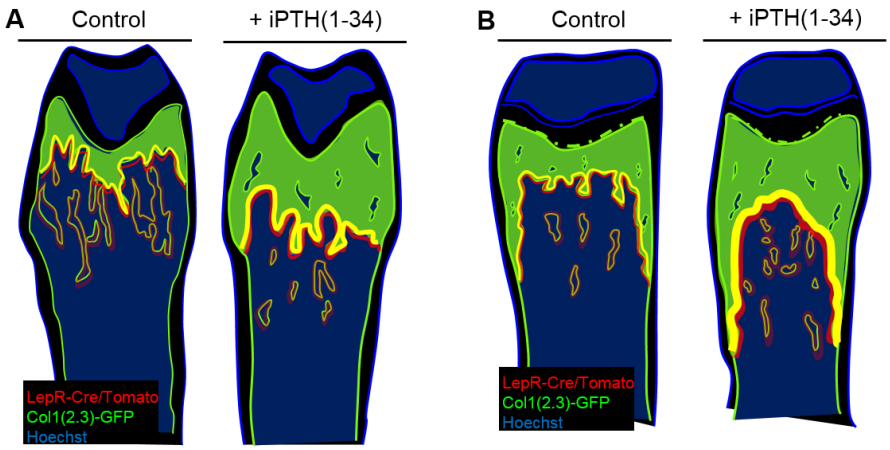

Figure 1. LepR$^+$MSPCs differentiated into mature osteoblasts by PTH(1-34) treatement.
Three to 6-week-old LepR-Cre/Tomato/Col1(2.3)-GFP mice were treated with vehicle or PTH(1-34) (80 mg/kg) at every 24 h (A) or 12 h (B) for 10 days. Mimic images of bone sections from vehicle and PTH(1-34) treated mice. Nuclei were visualized using Hoechst 33342 (blue). LepR-Cre/Tomato$^+$ Col1(2.3)-GFP$^+$ cells (yellow).

Table 2 Effect of PTH(1-34) treatment on osteoblastogenesis of LepR$^+$MSPCs

Parameters	PTH(1-34) Mean±SD
LepR-Cre/Tomato$^+$/Col1(2.3)-GFP$^+$ cells / mm^2	↑ *
LepR-Cre/Tomato$^+$/Col1(2.3)-GFP$^+$ cells / femur (%)	↑ *
LepR-Cre/Tomato$^+$/Col1(2.3)-GFP$^+$ cells ($\times 10^3$) / femur	↑ **

Three-week-old LepR-Cre/Tomato/Col1(2.3)-GFP mice were treated with vehicle or PTH(1-34) (80 mg/kg) at every 24 h for 10 days.Quantification of the number of LepR-Cre/Tomato$^+$Col1(2.3)-GFP$^+$ cells in an area of 2 mm^2 in 500 mm below from growth plate (first line) and the frequency (second line) and absolute number (third line) of LepR-Cre/Tomato$^+$Col1(2.3)-GFP$^+$cells analyzed by FACS. n=4–5. *$p < 0.05$, **$p < 0.01$. Data are represent-ed as mean ± SD.

Table 3 Effect of PTH(1-34) treatment on osteoblastogenesis of LepR$^+$MSPCs

Parameters	PTH(1-34) Mean±SD
LepR-Cre/Tomato$^+$/Col1(2.3)-GFP$^+$ cells / mm^2	↑ **

Six-week-old LepR-Cre/Tomato/Col1(2.3)-GFP mice were treated with vehicle or PTH(1-34) (80 mg/kg) at every 12 h for 10 days. Quantification of the number of LepR-Cre/Tomato$^+$Col1(2.3)-GFP$^+$ cells in an area of 2 mm^2 in 500 mm below from growth plate. n=5. ** $p < 0.01$. Data are represented as mean ± SD.

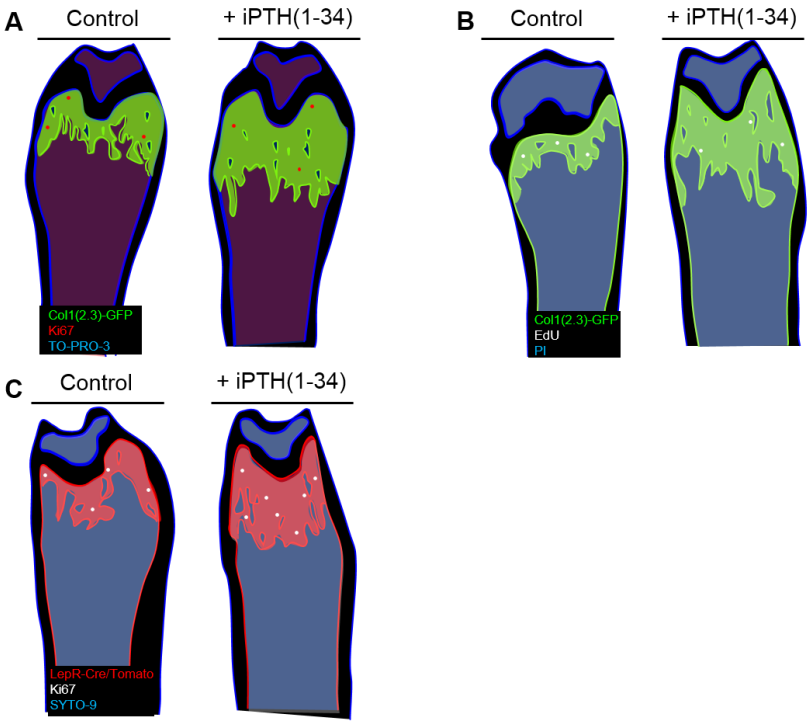

Figure 2. LepR$^+$MSPCs were induced cell cycle progression by PTH(1-34) treatment and differentiated into mature osteoblasts with cell cycle withdrawal.
Five to Eight-week-old Col1(2.3)-GFP (A.B) and LepR-Cre/Tomato mice (C) were treated with vehicle or PTH(1-34) (80 mg/kg/24 h) for 10 days. Mimic images of bone sections from vehicle and PTH(1-34) treated mice. Nuclei were visualized using TO-PRO-3 (blue)(A), propidium iodide (PI) (blue) (B) or SYTO-9 (blue) (C).

Table 4 Effect of PTH(1-34) treatment on the number of mature osteoblasts

Parameters	PTH(1-34) Mean±SD
Col1(2.3)-GFP$^+$ cells / mm^2	↑ ***

Six-week-old Col1(2.3)-GFP were treated with vehicle or PTH(1-34) (80 mg/kg/24 h) for 10 days. Quantification of the absolute number of Col1(2.3)-GFP$^+$ cells in an area of 1 mm^2 in 100 mm below from growth plate. n=6. $^{***}p < 0.001$. Data are shown as mean ±SD.

Table 5 Effect of PTH(1-34) treatment on the proliferation of mature osteoblasts

Parameters	PTH(1-34) Mean±SD
$Ki67^+$ $Col1(2.3)\text{-}GFP^+$ cells / mm^2	-- NS
$Ki67^-$ $Col1(2.3)\text{-}GFP^+$ cells / mm^2	↑ *

Six-week-old Col1(2.3)-GFP were treated with vehicle or PTH(1-34) (80 mg/kg/24 h) for 10 days. Quantification of the absolute number of $Ki67^+Col1(2.3)\text{-}GFP^+$ cells (first line) and $Ki67^-Col1(2.3)\text{-}GFP^+$ cells (second line) in an area of 1 mm^2 in 100 mm below from growth plate. n=7. $*p < 0.05$, NS: not significant. Data are shown as mean ± SD.

Table 6 Effect of PTH(1-34) treatment on the proliferation of mature osteoblasts

Parameters	PTH(1-34) Mean±SD
EdU^+ Col1(2.3)-GFP^+ cells / mm^2	-- NS
EdU^- Col1(2.3)-GFP^+ cells / mm^2	↑ **

Five-week-old Col1(2.3)-GFP were treated with vehicle or PTH(1-34) (80 mg/kg/24 h) for 10 days. Quantification of the absolute number of EdU^+Col1(2.3)-GFP^+ cells (first line) and EdU^-Col1(2.3)-GFP^+ cells (second line) in an area of 0.25 mm^2 under the growth plate. Two sections from mouse femur were used for the quantifications. n=3. $^{**}p < 0.01$, NS: not significant. Data are shown as mean ± SD.

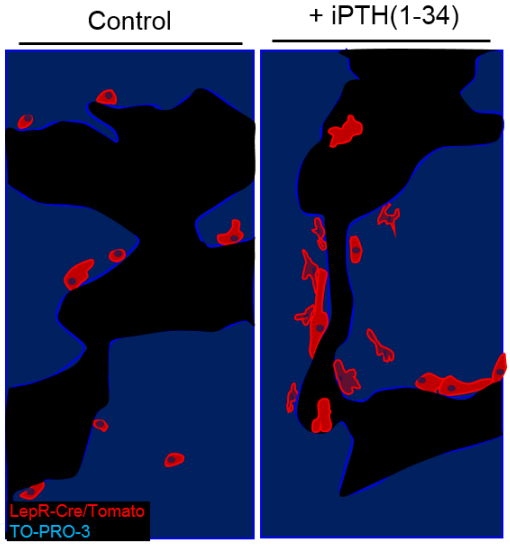

Figure 3. LepR-Cre/Tomato^{+} cells were increased near the bone surface in response to PTH(1-34) treatment.

Eight-week-old LepR-Cre/Tomato mice were treated with vehicle or iPTH(1-34) (80 mg/kg/24 h) for 10 days. Mimic images of bone sections. Nuclei were visualized with TO-PRO-3 (blue).

Table 7 Effect of PTH(1-34) treatment on the proliferation of LepR$^+$MSPCs

Parameters	PTH(1-34) Mean±SD
Ki67$^+$ LepR-Cre/Tomato$^+$ cells / mm^2	↑ **

Eight-week-old LepR-Cre/Tomato were treated with vehicle or PTH(1-34) (80 mg/kg/24 h) for 10 days. Quantification of the absolute number of Ki67$^+$LepR-Cre/Tomato$^+$ cells in an area of 0.25 mm^2 under the growth plate. n=10. $^{**}p < 0.01$. Data are shown as mean ± SD.

Table 8 Effect of PTH(1-34) treatment on the proliferation of LepR$^+$MSPCs

Parameters	PTH(1-34) Mean±SD
Ki67$^+$ LepR-Cre/Tomato$^+$ cells / femur (%)	↑ *

8-week-old LepR-Cre/Tomato were treated with vehicle or PTH(1-34) (80 mg/kg/24 h) for 10 days. Quantification of the frequency of Ki67$^+$ cells in LepR-Cre/Tomato$^+$ cells analyzed by FACS. n=8. $*p < 0.05$. Data are shown as mean ± SD.

Table 9 Effect of PTH(1-34) treatment on the expression levels of osteoblastic markers in LepR^{+}MSPCs

Parameters (relative mRNA)	PTH(1-34) Mean±SD
Col1a1	↑ ****
Sp7	↑ ****
Bglap	-- NS
Alpl	↓ ***

CD45^{-}Ter119^{-}CD31^{-}LepR^{+}Nestin-GFP^{+} BM stromal population was sorted from 2-year-old Nestin-GFP mice with or without PTH(1-34) treatment (80 mg/kg/24 h) for 10 days. Quantitative real-time PCR analysis for mRNA expression of osteoblastogenesis-related factors (Col1a1, Sp7, Bglap, Alpl). Whole BM cells from 3 mice in each group were mixed and use for cell sorting. ****p < 0.001, ****p < 0.0001,* NS: not significant. Data are shown as mean ± SD.

Table 10 Effect of PTH(1-34) treatment on the expression levels of adipocytic markers in $LepR^+$MSPCs

Parameters (relative mRNA)	PTH(1-34) Mean±SD
Pparg	↓ ***
Cebpb	↓ *
Zfp467	↓ ***
Fabp4	↑ ***

$CD45^-Ter119^-CD31^-LepR^+Nestin\text{-}GFP^+$ BM stromal population was sorted from 2-year-old Nestin-GFP mice with or without PTH(1-34) treatment (80 mg/kg/24 h) for 10 days. Quantitative real-time PCR analysis for mRNA expression of adipogenesis-related factors (Pparg, Cebpb, Zfp467, Fabp4). Whole BM cells from 3 mice in each group were mixed and use for cell sorting. $*p < 0.05$, $***p < 0.001$. Data are shown as mean ± SD.

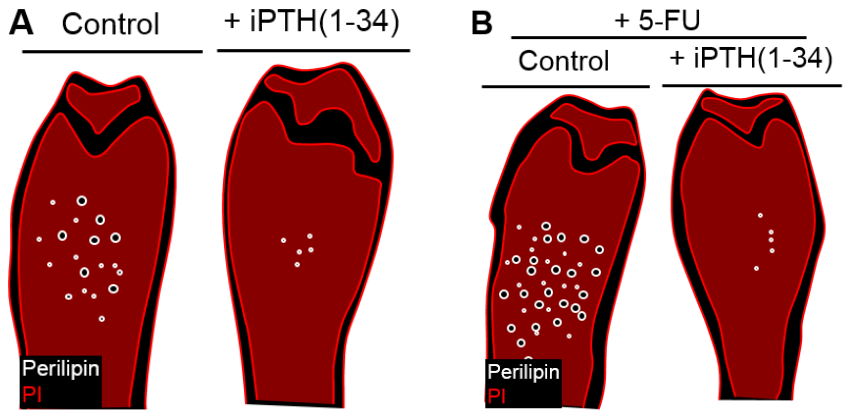

Figure 4. PTH(1-34) treatment suppressed adipocytic differentiation in BM cavity.
Six-week-old mice were treated with vehicle or iPTH(1-34) (80 mg/kg/24 h) for 10 days with (B) or without (A) 5-FU (250 mg/kg) pre-treatment. Mimic images of bone sections from vehicle and PTH(1-34) treated mice. Perilipin$^+$ adipocytes (white). Nuclei were visualized using PI (red).

Table 11 Effect of PTH(1-34) treatment on adipogenesis of MSPCs

Parameters	PTH(1-34) Mean±SD
Perilipin$^+$ adipocytes / mm^2	↓ *

Six-week-old mice were treated with vehicle or iPTH(1-34) (80 mg/kg/24 h) for 10 days. Quantification of the absolute number of Perilipin$^+$ adipocytes in an area of 2 mm^2 under the growth plate. n=4. $*p < 0.05$. Data are shown as mean ± SD.

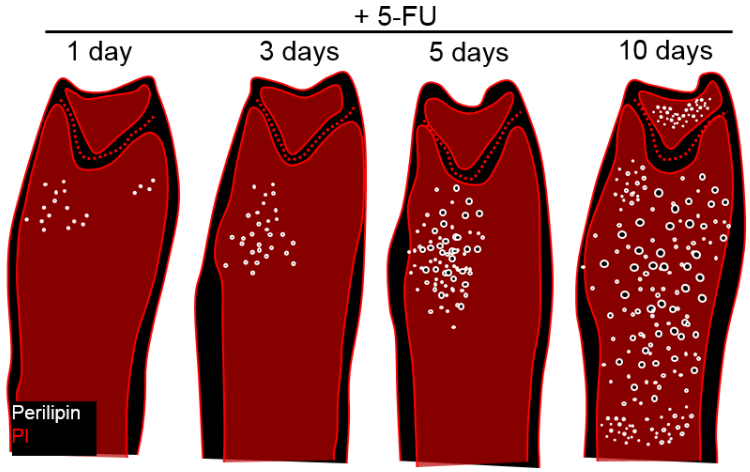

Figure 5. 5-FU injection induced adipocytic differentiation in BM cavity
Mimic images of bone sections on 5-FU (250 mg/kg) injected 6-week-old mice at the indicated time points stained with anti-Perilipin antibody (white). Nuclei were visualized by PI (red).

Table 12 Effect of PTH(1-34) treatment on 5-FU-induced adipogenesis of MSPCs

Parameters	PTH(1-34) Mean±SD
Perilipin$^+$ adipocytes / mm^2	↓ *

Six-week-old mice were treated with vehicle or iPTH(1-34) (80 mg/kg/24 h) for 10 days with 5-FU (250 mg/kg) pre-treatment. Quantification of the absolute number of Perilipin$^+$ adipocytes in an area of 4 mm^2 in 1 mm below from growth plate. n=4. $*p < 0.05$. Data are shown as mean ± SD.

Table 13 Effect of PTH(1-34) treatment on the morphometric parameters of bone tissue

Parameters (units)	PTH(1-34) Mean±SD
BV/TV (%)	↑ **
Tb.Th. (μm)	-- NS
Tb.N. (mm^{-1})	↑ ***
Tb.Sp. (μm)	↓ **

Six-week-old mice were treated with vehicle or iPTH(1-34) (80 mg/kg/24 h) for 10 days with 5-FU (250 mg/kg) pre-treatment. Quantification of bone parameters: BV/TV, bone volume over total volume; Tb.Th., trabecular thickness; TbN., trabecular number; Tb.Sp., trabecular separation. n=4. *$^{**}p < 0.01$, $^{***}p < 0.001$.* NS: not significant. Data are shown as mean ± SD.

Table 14 Effect of PTH(1-34) treatment on the cortical area in ovariectomized(OVX) mice

Parameters (unit)	Sham Mean±SD	OVX[a,] Mean±SD	OVX+PTH(60)[a,b] Mean±SD	OVX+PTH(20×3)[a,b] Mean±SD
Cortical area (%)		↓ ***	-- NS	-- NS
			↑ **	↑ ****

Six-month-old rats were ovariectomized or sham-operated and bled for 6 months to establish osteoporosis. Rats were treated with vehicle or PTH(1-34) [60 mg/kg/week: PTH(60) or 20 mg/kg × 3 times/week: PTH(20x3)] for 6 months. Quantification of cortical area. a: versus vehicle-treated sham group. b: versus vehicle-treated OVX group. n=7. ***p < 0.01, ***p < 0.001, ****p < 0.0001.* Data are shown as mean ± SD.

Table 15 Effect of PTH(1-34) treatment on the adipose tissue area in ovariectomized(OVX) mice

Parameters (unit)	Sham Mean±SD	OVX[a] Mean±SD	OVX+PTH(60)[a,b] Mean±SD	OVX+PTH(20×3)[a,b] Mean±SD
Adipose tissue area (%)		↑ *	-- NS	-- NS
			-- NS	↓ *

Six-month-old rats were ovariectomized or sham-operated and bled for 6 months to establish osteoporosis. Rats were treated with vehicle or PTH(1-34) [60 mg/kg/week: PTH(60) or 20 mg/kg × 3 times/week: PTH(20x3)] for 6 months. Quantification of adipose tissue area. a: versus vehicle-treated sham group. b: versus vehicle-treated OVX group. n=7. $^{**}p < 0.01$, NS: no significant. Data are shown as mean ± SD.

Figure 4

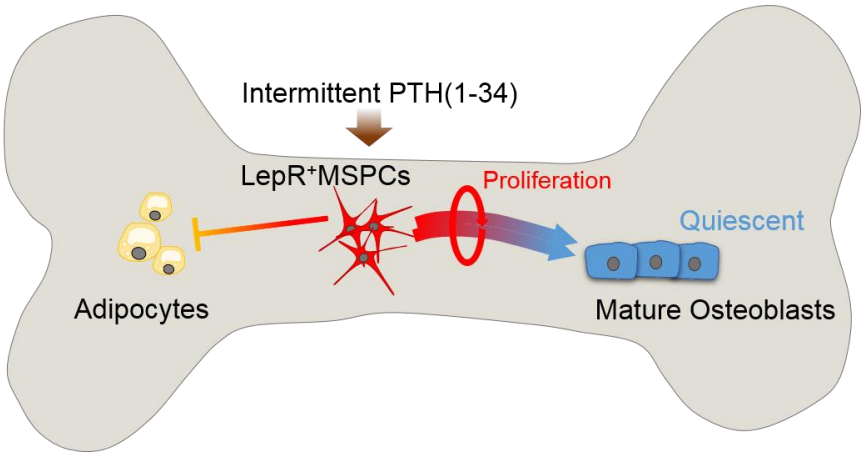

Figure 4. Effect of PTH(1-34) treatment on lineage differentiation of LepR$^+$MSPCs.
iPTH(1-34) treatment induces osteoblastogenesis of LepR$^+$MSPCs. In this process, LepR$^+$MSPCs proliferate and differentiate into mature osteoblasts through cell cycle withdrawal. In contrast, adipocytic differentiation is suppressed by iPTH(1-34) treatment suggesting that part of the bone anabolic effect of iPTH(1-34) treatment is exerted by lineage switching toward osteoblasts from adipocytes.

5. DISCUSSION

Genetic lineage tracing analyses provide a way to identify the BM-MSPC population and their progeny *in vivo*. This experimental approach also permitted to observation of the effect of iPTH treatment on lineage differentiation of BM-MSPCs. Here, we demonstrated that the BM-MSPC population proliferated after iPTH treatment, and subsequently became mature osteoblasts in a quiescent state. Concomitantly, adipocytic differentiation was attenuated in this BM milieu, suggesting that iPTH treatment switches lineage differentiation of BM-MSPCs towered osteoblasts from adipocytes.

There is evidence suggesting that iPTH treatment increases the number of mature osteoblasts, however, the mechanism of this process is still controversial [33]. Previous studies provided *in vivo* data that showed iPTH treatment attenuated apoptosis of mature osteoblasts [37, 38] or activated quiescent bone lining cells [39, 40], resulting in increased of mature osteoblasts. Consistent with this, our results demonstrated that mature osteoblasts increased after iPTH treatment, despite the fact that Ki67 expression was rarely observed in their nuclei. These findings indicated that PTH-induced expansion of mature osteoblasts was not mediated by their proliferation. Furthermore, previous *in vitro* studies demonstrated that PTH treatment induced growth arrest in mature osteoblasts by mediating the suppression of Cyclin D1, which is required for cell cycle progression [41, 42]. As oppose to mature osteoblasts, our results indicated that LepR^{+}MSPCs proliferate in response to iPTH treatment, which was consistent with previous data in which PTH increases cell cycle progression of immature osteoblasts [16, 18]. Of note, it has been suggested that PTH-exerted cell-cycle regulation differs depending on the differentiation stage of osteoblasts [17]. LepR^{+}MSPCs differentiate into mature osteoblasts by iPTH treatment, as demonstrated by our genetic lineage tracing analyses. Altogether, these results suggested that the expansion and osteoblastic differentiation of immature stromal population are at least one of the mechanisms responsible for increased mature osteoblasts by iPTH treatment.

Our data demonstrated that markers for osteoblasts, Col1a1 and Osx/SP7, were increased, but adipocytic markers, Pparg, Cenpb and Zfp467, were decreased in purified BM-MSPC populations after iPTH treatment. In accordance with these results, Perilipin$^+$ BM adipocytes were significantly decreased in these conditions. Additionally, iPTH treatment suppressed 5-FU or OVX-induced adipocytogenesis in the BM cavity. It is noteworthy that the bone volume was increased in this situation. Consistently, resent reports indicated that BM adipose tissue was reduced in idiopathic osteoporotic patients following PTH therapy [30]. Altogether, these results suggested that PTH provoked stromal lineage switching toward osteoblasts from adipocytes, and the effect was exerted on the BM-MSPC population, but not on osteoblasts or adipocytes. However, the osteoblastic marker ALP or adipocytic marker Fabp4 were exactly showed opposite behavior in our real-time PCR analysis. Of note, recent reports demonstrated that BM adipocytogenesis was accelerated after the discontinuation of iPTH treatment [22]. The experimental mice used for our real-time PCR analysis was sacrificed 24 hours after final PTH injection, and the serum half-life of PTH(1–34) is within 15 min [43, 44]. Therefore, the adipocytic differentiation pathway might already be induced in our sorted BM-MSPC population.

The LepR-Cre-marked BM stromal population was suggested to be maintained in a quiescent state at steady-state [5]. Our Ki67 immunostaining approach revealed that the proliferating LepR$^+$MSPCs were observed in the vicinity of the bone surface as multilayered cells after iPTH treatment. Stromal colony forming potential (known as colony-forming unit-fibroblasts [CFU-F]) are considered as the self-renewal capacity of stem cells [45]. A previous study demonstrated that iPTH treatment increased CFU-F activity in endosteal stromal progenitor but not those in the central BM [46]. These results may indicate that iPTH induces self-renew to replenish differentiated LepR$^+$MSPCs into osteoblasts in the endosteum. It is noteworthy that PTH-induced proliferative activity on LepR$^+$MSPCs was exerted only on the bone surface but not in the central area of the BM cavity, although the LepR-Cre marked stromal population was suggested to be localized to the whole BM cavity adjacent to the sinusoid [47]. The CFU-F assay revealed that the stem cell capacity was enriched in the area near by the bone surface in normal mice [46],

suggesting that the regulatory milieu for stem cell maintenance may be localized there. Further analysis of the mechanistic details of the regulatory BM environment for the stromal population will provide valuable information for therapeutic targeting for bone loss associated with osteoporosis and aging.

6. REFERENCES

1. Xiong J, O'Brien CA (2012) Osteocyte RANKL: new insights into the control of bone remodeling. *J Bone Miner Res* 27 : 499-505.
2. Seeman E, Martin TJ (2015) Co-administration of antiresorptive and anabolic agents: a missed opportunity. *J Bone Miner Res* 30 : 753-764.
3. Park D, Spencer JA, Koh BI, Kobayashi T, Fujisaki J, Clemens TL, Lin CP, Kronenberg HM, Scadden DT (2012) Endogenous bone marrow MSCs are dynamic, fate-restricted participants in bone maintenance and regeneration. *Cell Stem Cell* 10 : 259-272.
4. Mizoguchi T, Pinho S, Ahmed J, Kunisaki Y, Hanoun M, Mendelson A, Ono N, Kronenberg HM, Frenette PS (2014) Osterix marks distinct waves of primitive and definitive stromal progenitors during bone marrow development. *Dev Cell.* 29 : 340-349.
5. Zhou BO, Yue R, Murphy MM, Peyer JG, Morrison SJ (2014) Leptin-receptor-expressing mesenchymal stromal cells represent the main source of bone formed by adult bone marrow. *Cell Stem Cell* 15 : 154-168.
6. Kunisaki Y, Bruns I, Scheiermann C, Ahmed J, Pinho S, Zhang D, Mizoguchi T, Wei Q, Lucas D, Ito K, Mar JC, Bergman A, Frenette PS (2013) Arteriolar niches maintain haematopoietic stem cell quiescence. *Nature* 502 : 637-643.
7. Pinho S, Lacombe J, Hanoun M, Mizoguchi T, Bruns I, Kunisaki Y, et al. (2013) PDGFRalpha and CD51 mark human nestin+ sphere-forming mesenchymal stem cells capable of hematopoietic progenitor cell expansion. *J Exp Med* 210 : 1351-1367
8. Ding L, Morrison SJ (2013) Haematopoietic stem cells and early lymphoid progenitors occupy distinct bone marrow niches. *Nature* 495 : 231-235.
9. Omatsu Y, Seike M, Sugiyama T, Kume T, Nagasawa T (2014) Foxc1 is a critical regulator of haematopoietic stem/progenitor cell niche formation. *Nature* 508 : 536-540
10. Yue R, Zhou BO, Shimada IS, Zhao Z, Morrison SJ (2016) Leptin Receptor Promotes Adipogenesis and Reduces Osteogenesis by Regulating Mesenchymal Stromal Cells in Adult Bone Marrow. *Cell Stem Cell* 18 : 782-796.

11. Ono N, Ono W, Nagasawa T, Kronenberg HM (2014) A subset of chondrogenic cells provides early mesenchymal progenitors in growing bones. *Nat Cell Biol* 16 : 1157-1167.
12. Shi Y, He G, Lee WC, McKenzie JA, Silva MJ, Long F (2017) Gli1 identifies osteogenic progenitors for bone formation and fracture repair. *Nat Commun* 8 : 2043.
13. Li L, Clevers H (2010) Coexistence of quiescent and active adult stem cells in mammals. *Science* 327 : 542-545.
14. Nakamura-Ishizu A, Takizawa H, Suda T (2014) The analysis, roles and regulation of quiescence in hematopoietic stem cells. *Development* 141 : 4656-4666.
15. Rumman M, Dhawan J, Kassem M (2015) Concise Review: Quiescence in Adult Stem Cells: Biological Significance and Relevance to Tissue Regeneration. *Stem Cells* 33 : 2903-2912.
16. Lotinun S, Sibonga JD, Turner RT (2005) Evidence that the cells responsible for marrow fibrosis in a rat model for hyperparathyroidism are preosteoblasts. *Endocrinology* 146 : 4074-4081.
17. Datta NS, Pettway GJ, Chen C, Koh AJ, McCauley LK (2007) Cyclin D1 as a target for the proliferative effects of PTH and PTHrP in early osteoblastic cells. *J Bone Miner Res* 22 : 951-964.
18. Luiz de Freitas PH, Li M, Ninomiya T, Nakamura M, Ubaidus S, Oda K, Udagawa N, Maeda T, Takagi R, Amizuka N (2009) Intermittent PTH administration stimulates pre-osteoblastic proliferation without leading to enhanced bone formation in osteoclast-less c-fos(-/-) mice. *J Bone Miner Res* 24 : 1586-1597.
19. Ogura K, Iimura T, Makino Y, Sugie-Oya A, Takakura A, Takao-Kawabata R, Ishizuya T, Moriyama K, Yamaguchi A (2016) Short-term intermittent administration of parathyroid hormone facilitates osteogenesis by different mechanisms in cancellous and cortical bone. *Bone Rep* 5 : 7-14.
20. Yamamoto T, Hasegawa T, Sasaki M, Hongo H, Tsuboi K, Shimizu T, Ota M, Haraguchi M, Takahata M, Oda K, Luiz de Freitas PH, Takakura A, Takao-Kawabata R, Isogai Y, Amizuka N (2016) Frequency of teriparatide administra-

tion affects the histological pattern of bone formation in young adult male mice. *Endocrinology* 157 : 2604-2620.

21. Yang M, Arai A, Udagawa N, Hiraga T, Lijuan Z, Ito S, Komori T, Moriishi T, Matsuo K, Shimoda K, Zahalka AH, Kobayashi Y, Takahashi N, Mizoguchi T (2017) Osteogenic Factor Runx2 Marks a Subset of Leptin Receptor-Positive Cells that Sit Atop the Bone Marrow Stromal Cell Hierarchy. *Sci Rep* 7(1) : 4928.
22. Balani DH, Ono N, Kronenberg HM (2017) Parathyroid hormone regulates fates of murine osteoblast precursors in vivo. *J Clin Invest* 127 : 3327-3338.
23. Meunier P, Aaron J, Edouard C, Vignon G (1971) Osteoporosis and the replacement of cell populations of the marrow by adipose tissue. A quantitative study of 84 iliac bone biopsies. *Clin Orthop Relat Res* 80 : 147-154.
24. Rosen CJ, Bouxsein ML (2006) Mechanisms of disease: is osteoporosis the obesity of bone? *Nat Clin Pract Rheumatol* 2 : 35-43.
25. Georgiou KR, Hui SK, Xian CJ (2012) Regulatory pathways associated with bone loss and bone marrow adiposity caused by aging, chemotherapy, glucocorticoid therapy and radiotherapy. *Am J Stem Cells* 1 : 205-224.
26. Ishizuya T, Yokose S, Hori M, Noda T, Suda T, Yoshiki S, Yamaguchi A (1997) Parathyroid hormone exerts disparate effects on osteoblast differentiation depending on exposure time in rat osteoblastic cells. *J Clin Invest* 99 :2961-2970.
27. Chan GK, Deckelbaum RA, Bolivar I, Goltzman D, Karaplis AC (2001) PTHrP inhibits adipocyte differentiation by down-regulating PPAR gamma activity via a MAPK-dependent pathway. *Endocrinology* 142 : 4900-4909.
28. Chan GK, Miao D, Deckelbaum R, Bolivar I, Karaplis A, Goltzman D (2003) Parathyroid hormone-related peptide interacts with bone morphogenetic protein 2 to increase osteoblastogenesis and decrease adipogenesis in pluripotent C3H10T 1/2 mesenchymal cells. *Endocrinology* 144 : 5511-5520.
29. Amizuka N, Karaplis AC, Henderson JE, Warshawsky H, Lipman ML, Matsuki Y, Ejiri S, Tanaka M, Izumi N, Ozawa H, Goltzman D (1996) Haploinsufficiency of parathyroid hormone-related peptide (PTHrP) results in abnormal postnatal bone development. *Dev Biol* 175 : 166-176.
30. Fan Y, Hanai JI, Le PT, Bi R, Maridas D, DeMambro V, Figueroa CA, Kir S, Zhou X, Mannstadt M, Baron R, Bronson RT, Horowitz MC, Wu JY, Bilezikian JP,

Dempster DW, Rosen CJ, Lanske B (2017) Parathyroid Hormone Directs Bone Marrow Mesenchymal Cell Fate. *Cell Metab* 25 : 661-672.

31. Matsuo K, Kuroda Y, Nango N, Shimoda K, Kubota Y, Ema M, Bakiri L, Wagner EF, Takeda Y, Yashiro W, Momose A (2015) Osteogenic capillaries orchestrate growth plate-independent ossification of the malleus. *Development* 142 : 3912-3920.
32. Alexander JM, Bab I, Fish S, Muller R, Uchiyama T, Gronowicz G, Nahounou M, Zhao Q, White DW, Chorev M, Gazit D, Rosenblatt M (2001) Human parathyroid hormone 1-34 reverses bone loss in ovariectomized mice. *J Bone Miner Res* 16 : 1665-1673.
33. Jilka RL (2007) Molecular and cellular mechanisms of the anabolic effect of intermittent PTH. *Bone* 40 : 1434-1446.
34. Bianco P, Costantini M, Dearden LC, Bonucci E (1988) Alkaline phosphatase positive precursors of adipocytes in the human bone marrow. *Br J Haematol* 68 : 401-403.
35. Omatsu Y, Sugiyama T, Kohara H, Kondoh G, Fujii N, Kohno K, Nagasawa T (2010) The essential functions of adipo-osteogenic progenitors as the hematopoietic stem and progenitor cell niche. *Immunity* 33 : 387-399.
36. Devlin MJ, Rosen CJ (2015) The bone-fat interface: basic and clinical implications of marrow adiposity. *Lancet Diabetes Endocrinol* 3 : 141-147.
37. Jilka RL, Weinstein RS, Bellido T, Roberson P, Parfitt AM, Manolagas SC (1999) Increased bone formation by prevention of osteoblast apoptosis with parathyroid hormone. *J Clin Invest* 104 : 439-446.
38. Bellido T, Ali AA, Plotkin LI, Fu Q, Gubrij I, Roberson PK, Weinstein RS, O'Brien CA, Manolagas SC, Jilka RL (2003) Proteasomal degradation of Runx2 shortens parathyroid hormone-induced anti-apoptotic signaling in osteoblasts. A putative explanation for why intermittent administration is needed for bone anabolism. *J Biol Chem* 278 : 50259-50272.
39. Leaffer D, Sweeney M, Kellerman LA, Avnur Z, Krstenansky JL, Vickery BH, Caulfield JP (1995) Modulation of osteogenic cell ultrastructure by RS-23581, an analog of human parathyroid hormone (PTH)-related peptide-(1-34), and bovine PTH-(1-34). *Endocrinology* 136 : 3624-3631.

40. Kim SW, Pajevic PD, Selig M, Barry KJ, Yang JY, Shin CS, Baek WY, Kim JE, Kronenberg HM (2012) Intermittent parathyroid hormone administration converts quiescent lining cells to active osteoblasts. *J Bone Miner Res* 27 : 2075-2084.
41. Datta NS, Chen C, Berry JE, McCauley LK (2005) PTHrP signaling targets cyclin D1 and induces osteoblastic cell growth arrest. *J Bone Miner Re*s 20 : 1051-1064.
42. Qin L, Li X, Ko JK, Partridge NC (2005) Parathyroid hormone uses multiple mechanisms to arrest the cell cycle progression of osteoblastic cells from G1 to S phase. *J Biol Chem* 280 : 3104-3111.
43. Shimizu M, Joyashiki E, Noda H, Watanabe T, Okazaki M, Nagayasu M, Adachi K, Tamura T, Potts JT Jr, Gardella TJ, Kawabe Y (2016) Pharmacodynamic Actions of a Long-Acting PTH Analog (LA-PTH) in Thyroparathyroidectomized (TPTX) Rats and Normal Monkeys. *J Bone Miner Res* 31 : 1405-1412
44. Tamura T, Noda H, Joyashiki E, Hoshino M, Watanabe T, Kinosaki M, Nishimura Y, Esaki T, Ogawa K, Miyake T, Arai S, Shimizu M, Kitamura H, Sato H, Kawabe Y. (2016) Identification of an orally active small-molecule PTHR1 agonist for the treatment of hypoparathyroidism. *Nat Commun* 7 : 13384.
45. Frenette PS, Pinho S, Lucas D, Scheiermann C (2013) Mesenchymal stem cell: keystone of the hematopoietic stem cell niche and a stepping-stone for regenerative medicine. *Annu Rev Immunol* 31 : 285-316.
46. Siclari VA, Zhu J, Akiyama K, Liu F, Zhang X, Chandra A, Nah HD, Shi S, Qin L (2013) Mesenchymal progenitors residing close to the bone surface are functionally distinct from those in the central bone marrow. *Bone* 53 : 575-86.
47. Ding L, Saunders TL, Enikolopov G, Morrison SJ (2012) Endothelial and perivascular cells maintain haematopoietic stem cells. *Nature* 481 : 457-462.
48. Mignone JL, Kukekov V, Chiang AS, Steindler D, Enikolopov G (2004) Neural stem and progenitor cells in nestin-GFP transgenic mice. *J Comp Neurol* 469 : 311-324.
49. Mignone J, Peunova N, Enikolopov G (2016) Nestin-Based Reporter Transgenic Mouse Lines. *Methods Mol Biol* 1453: 7-14.
50. Kawamoto T, Shimizu M (2000) A method for preparing 2- to 50-micron-thick fresh-frozen sections of large samples and undecalcified hard tissues. *Histochemistry and cell biology* 113 : 331-339.

51. Takao-Kawabata R, Isogai Y, Takakura A, Shimazu Y, Sugimoto E, Nakazono O, Ikegaki I, Kuriyama H, Tanaka S, Oda H, Ishizuya T (2015) Three-times-weekly administration of teriparatide improves vertebral and peripheral bone density, microarchitecture, and mechanical properties without accelerating bone resorption in ovariectomized rats. *Calcif Tissue Int* 97 :156-168

ACKNOWLEDGMENTS

I would like to express my sincere gratitude to my supervisors Dr. T. Mizoguchi & Dr. A. Arai for providing their invaluable guidance, comments and suggestions throughout the course of the project. I would specially thank to Dr. N. Takahashi and Dr. N. Udagawa for constantly motivating me to work harder. This project would not have completed without their enormous help and worthy experiment.

I also grateful to L. Zhao, D. Nishda and A. Iwadare for academic support and friendship. I thank to all the teachers and colleagues from Division of Hard Tissue Research of MDU for showing patience in my work and helping me develop my ideas.

Finally, I would like to acknowledge with gratitude, the support and love of my family – my parents, Mr. Yang and Ms. Lu; my aunt, Dr. Yang; my uncle, Dr. Li and my cousin, Wenzhu and Younan.